Research Square

Preprints are preliminary reports that have not undergone peer review.
They should not be considered conclusive, used to inform clinical practice,
or referenced by the media as validated information.

Biomolecular Interaction, Antibacterial and Anticancer Activities of Organometallic Re(I) Complexes with 5-(2-butyl-5-chloro-1H-imidazol-4-yl)-1,3-diaryl-4,5-dihydro-1H-pyrazole

Reena R. Varma
Sardar Patel University
Juhee G. Pandya
Sardar Patel University
Foram U. Vaidya
Indian Institute of Advanced Research
Chandramani Pathak
Amity University Haryana
Milan P. Dhaduk
Sardar Patel University
Ravi A. Dabhi
Sardar Patel University
Bhupesh S. Bhatt
Sardar Patel University
Mohan N. Patel (jeenen@gmail.com)
Sardar Patel University https://orcid.org/0000-0001-9016-9245

Research Article

Keywords: Organometallic Re(I), Imidazole-pyrazoline heterocyclic compounds, Cell Viability, Spectroscopy, Reactive Oxygen Species

Posted Date: April 22nd, 2021

DOI: https://doi.org/10.21203/rs.3.rs-430873/v1

License: This work is licensed under a Creative Commons Attribution 4.0 International License.
Read Full License

Abstract

Organometallic rhenium(I) complexes (I-VI) using substituted 5-(2-butyl-5-chloro-1H-imidazol-4-yl)-1,3-diaryl-4,5-dihydro-1H-pyrazole have been synthesized and characterised by spectroscopic method. For evaluation of HOMO-LUMO energy gap, estimation of bond angle, bond length data and Mulliken charge analysis DFT studies were performed. The complexes (I-VI) can be generated by bis-heterocyclic ligand followed by metal chelation. The interactions between synthesised compounds and double stranded DNA (HS DNA) was carried out by viscosity measurements, absorption titration, and gel electrophoresis gives information about modes of binding and the nucleolytic efficiency of compounds. Groove binding was suggested as the most possible mode and the DNA-binding (K_b) constants of the complexes were calculated. Electronic spectra and conductivity measurement confirm the different transition, and non-electrolytic nature of the metal complexes. Thermodynamic parameter ΔG^0 value ranging from -7227.0 to -9463.0 J/mole^{o}K. According to the thermodynamic parameter, the main binding force could be judged. *In vivo* and *In vitro* cytotoxicity against the eukaryotic and prokaryotic cells gives toxic nature of the synthesised compounds. An antimicrobial study was carried out by estimating MIC (Minimum Inhibitory Concentration) against two Gram-positive and three Gram-negative bacteria. All compounds found effective against *S. cerevisiae* which is confirmed by enhancing ROS production and DNA damage show by gel electrophoresis as compared to untreated yeast cell culture and DMSO.

1. Introduction

Metal plays an important role in the function of enzymes and proteins. For enhancing the biological activities, researchers are focussing on metal compounds [1–5], and the metal carbonyls are important for pharmaceutical and diagnosis. Metal carbonyls are coordination complexes of transition metals having carbon monoxide as a ligand. The substitution of carbon monoxide (CO) ligands can be induced thermally or photo chemically by donor ligands. In the last decade, the use of CO as a cytoprotective and homeostatic molecule has received increasing attention in medicine due to its documented beneficial therapeutic effects [6, 7]. There are three main areas where CO is evaluated as a clinically valuable medical agent like inflammation, cardiovascular diseases and organ preservation and transplantation [8]. Researchers have synthesize various transition metal carbonyl complexes for pro-drugs, which eventually deliver CO to biological targets and enhancing their effect [9, 10]. β^- -Emitter of rhenium ^{188}Re ($t_{1/2}$ = 16.9 h, E_{max} = 2.1 MeV, ^{186}Re ($t_{1/2}$ = 89.2 h, E_{max} = 1.1 MeV) having less half time and effective energy used in the treatment of cancerous cells and kill the cancer tissue [11].

Eprosartan and losartan having similar basic moiety with our synthesized compounds (Fig. 1). The presence of two aryl rings, the imidazole -NH and either a good electron withdrawing group or an aldehyde or amino group in bis heterocycles 5-(2-butyl-5-chloro-1H-imidazol-4-yl) [12], and 4,5-dihydro-1H-pyrazole moiety which gives good pharmacological and diagnostic application and metal chelation enhance the biological activity.

These all encouraged us to synthesize compounds containing bis-heterocyclic imidazole- pyrazoline moiety that chelated with the rhenium metal and evaluate their anti-yeast and anti-cancer activity. In continuation of our earlier work [13], in this study, our main focus is to enhance the anticancer activity of rhenium(I) complexes, DNA-binding affinities of synthesized compounds and imperative changes in some related properties. Thoughtful features that contribute to the recognition of DNA by metal based drugs or small molecules is crucial for the enhancement of drugs targeted at DNA. Based on the assessment of these inspections and the persistence of the research work on bioactive heterocyclic ligands and its complexes, their design and potential applications are anticipated.

2. Results And Discussion

2.1 ^{1}H NMR, ^{13}C-APT, IR, elemental, magnetic moments, conductance measurements, and electronic spectral analysis

^{1}H-NMR data of compounds show signals in 0.7–1.5 δ ppm range, which confirms aliphatic carbon chain present in molecule. Doublet of doublet signal observed at 3.0–5.0 δ ppm confirms methylene group in pyrazoline ring. The signal between 6.0–8.0 δ ppm confirms aromatic ring protons, and peak at ~ 12.0 δ ppm stands for –NH of imidazole ring.^{13}C-APT data of compounds show signals at 22–30 δ ppm confirms aliphatic chain present in imidazole ring, and signals at 180–190 δ ppm value confirms carbonyl groups in complexes.

Results of the FT-IR spectra of bis hetrocycles imidazole-pyrazoline derivatives (L^1-L^6) show the peak at ~ 3310–3550 due to v-NH secondary amine. present in the imidazole ring, peak at ~ 2954 cm^{-1} due to vC-H stretching band present in side chain of imidazole ring, peak at 2930 cm^{-1} due to v(= C-H)ar, and peak at ~ 2354 cm^{-1} due to vC-N stretching for imidazole ring. Pyrazoline ring contain v(> C = N) stretching bands observed at 1463–1564 cm^{-1} and peak at ~ 590–620 cm^{-1} shows carbon-halogen bond present in ligand. Peak at ~ 977–1062 cm^{-1} indicate presence of para substituted benzene ring, peak at ~ 1569 cm^{-1} and ~ 1315 cm^{-1} due to v(C = N) and v(C = C) stretching, but for complexes (I-VI), v(> C = N) bands are shifted to higher frequencies at around 1596 cm^{-1}. In complexes, the v(Re -N) bands are appeared at around 570–578 cm^{1} [14]. Infrared spectra for all compound showed carbonyl peaks between 2020–1875 cm^{-1} [15].

Magnetic moments value of rhenium(I) complexes is found to be zero because of the μ_{eff}. values indicate it has no unpaired electron i.e. low spin t_2g^6 eg^0 configuration resulting that all rhenium(I) complexes are diamagnetic in nature and also suggest that metal complex of rhenium is in + 1 oxidation state. Molar conductance values of all low spin rhenium(I) complexes are found in the range of 2.03-20.0 $\Omega^{-1}cm^2mol^{-1}$. It suggests that Re(I) complexes are non-ionic and non-electrolytic and no counter ions surrounding the coordination sphere. Three bands observed in electronic spectrum: one band ranging in

430-450.5 nm region assign to MLCT, second ranging from 340-356.5 nm region attributed to n–π* and third ranging from 260–290 assign to π–π*. From these Re(I) complexes exhibit an octahedral geometry [16].

2.2 Computational analysis

All density functional theory (DFT) calculations were performed using the Gaussian-09 program package. The DFT/B3LYP (Becke three-parameter Lee-Yang-Parr) method with LanL2DZ basis set is used to determine optimized geometry in which bond lengths and bond angles are calculated. The optimized electronic structure, optimized bond length and bond angles of all complexes are shown in supplementary material 3.

2.2.1 HOMO-LUMO energy

The frontier molecular orbitals (FMO), HOMO, and LUMO play a significant role in the study of electrical and optical properties. The HOMO (highest occupied molecular orbital) and LUMO (lowest unoccupied molecular orbital) give information about the interaction of a molecule with other species. The HOMO signifies the ability to donate an electron, and the LUMO to accept an electron. A molecule with a small difference in the orbital energy is usually more reactive. Among numerous other uses, the energy gap (Eg) between HOMO and LUMO is used to predict the activity and intramolecular charge transfer in organic as well as inorganic molecules with conjugated π bonds. The energy gap between HOMO-LUMO orbitals of the complexes I - V are 1.8251 eV, 1.8648 eV, 1.7878 eV, 1.8022 eV, and 1.8240 eV, respectively in the gaseous phase. From Fig. 1, it can be concluded that HOMO is evenly distributed in the central Re atom through the carbonyl group whereas LUMO is distributed in the ligand's moiety. HOMO-LUMO orbital structures of all the complexes are shown in supplementary material 3.

2.2.2 Mulliken Population analysis:

The atomic charge can be determined by Mulliken population analysis (MPA) of the complexes. The bonding ability of a molecule depends on the electronic charge on the atoms. The analysis of complex-I expresses that the atoms C12 (-0.41226), N9(-0.30893), N18 (-0.2879), O8 (-0.22596) display highest electronegativity and atoms C11 (0.724759), C21 (0.39019), C30 (0.32585), C5 (0.129583) display highest electropositivity. In complex-II, the atoms N9 (-0.30994), C12 (-0.41065), N18 (-0.28387), O8 (-0.22043), and N19(-0.15802) display highest electronegativity and atoms C11 (0.7552), C21(0.423596), C30(0.334657), C5(0.134672), C7 (0.131936) show highest electropositivity. In complex-III, the atoms C12 (-0.41114), N9 (-0.2992), N18 (-0.27704), C28 (-0.24569), O4 (-0.22439), show highest electronegativity and atoms C11 (0.720572), C21 (0.41703), C31 (0.325843), C5 (0.132666) show highest electropositivity. In complex-IV, the atoms C12 (-0.4126), N9 (-0.30221), O8 (-0.23143), O4 (-0.22949), C22 (-0.22237) show highest electronegativity and atoms C11(0.720233), C21 (0.471634), C30 (0.346886), C37 (0.339673), show highest electropositivity. In complex-V, the atoms C12 (-0.41337), N9 (-0.30706), N18 (-0.28465), O8 (-0. 18046), O4 (-0.22918) show highest electronegativity and atoms C11 (0.722708), C21 (0.403959), C28 (0.425643), C30 (0.328268) show highest electropositivity. In complex-VI, the atoms C12 (-0.40394),

N18 (-0.2642), O32 (-0.2185), O33 (-0.22133), show highest electronegativity and atoms C11 (0.716165), C21 (0.446585), C28 (0.352179), C34 (0.334441) show highest electropositivity. All the values and bar-chart analysis of Mulliken charges for all complexes are shown in the supplementary material 3.

2.3 Biological applications of synthesized ligands and complexes

2.3.1 Antiproliferation study

The development of drug resistance either intrinsically or as a result of treatment is a major challenge in cancer therapy. So design and synthesis of novel therapeutic compounds which can overcome resistance has become necessary to improve cancer survival rate. MTT assay was carried out for synthesised complexes on HCT 116 cell line. Metal carbonyls show good anticancer activity as compared to other metal complexes as shows in Table 1. The decreasing order of IC_{50} values is **II > III = IV = V > I > cisplatin > VI > oxaliplatine > carboplatin**. As the concentration increases the % cell proliferation is deceases means number of cells inhibit the tumor cells (Fig. 4). Above 500 µg/mL concentration solution becomes turbid, coloration and visibility not seen properly, from these we conclude synthesised complexes gives good anticancer activity. These approach to the metal complexes having carbon monoxide (CO) and heterocyclic compound with three to four bond distance presence of hetero atom chelated with rhenium metal is promising in terms of enhancing anticancer activity.

Table 1
IC_{50} values of complexes with the standard anticancer drugs

Compound	IC_{50} Value (µg/mL)
I	15.11
II	‹ 10
III	12.42
IV	12.42
V	12.42
VI	20.5
Cisplatin	15.49
Carboplatin	> 111.37
Oxaliplatin	22.66

2.3.2 Anti yeast activity using S. cerevisiae cells

The cellular level cytotoxicity or potency of ligands L^1-L^6 and complexes I-VI by its effect on *Saccharomyces Cerevisiae* cells in terms of % viability. The *in-vitro* cytotoxicity was found to vary with the type of substituent present and concentrations of the synthesized complexes i.e. 20 µg/mL, 40 µg/mL, 60 µg/mL, 80 µg/mL, 100 µg/mL, respectively. The Effect of compounds on the yeast cells shown in Fig. 5. From the result as concentration of compound increases, cytotoxic nature increases and % viability decreases (Fig. 6). Prohibiting capability of complexes is higher than the ligands. Complex-IV is most toxic to cell than the all the compound's and comparable with amphotericin B, while complex-II having higher cytotoxic than ciprofloxacin, norfloxacine and terbinafine. Amongst all the synthesized compound complex-IV and II are more cytotoxic in nature. The increasing order of % viability of compounds are **ciprofloxacin < L^6 < norfloxacine < L^1 < L^5 < L^3 < L^2 < I < VI < III < V < terbinafine < L^4 < II < IV ≈ amphotericin B**.

2.3.3 In vitro brine shrimp lethality bioassay (BSLB)

The BSLB is a subsidiary method for calculating toxic nature of synthesized compounds and also indicate the pharmacological activities of the compounds. It is widely used in the bioassay for the bioactive compounds [17]. The method is inexpensive, reliable, rapid, and economical. The result for the toxicity means lethality in terms of death of the larvae. As the concentration increases number of dead naupalli increase shows in Fig. 7. A plot of the log of the sample's concentration versus percentage (%) of mortality showed a linear correlation. The synthesized complexes have more death rate of naupalli as compared to the synthesized ligands. The increasing mortality rate are **L^4 < L^3 < L^2 < IV < III < L^6 < II < L^1 < L^5 ≈ VI < I < V**. From the graph LC_{50} value of the compounds was calculated, complex-V is the most potent amongst all the compounds.

2.3.4 In vitro antimicrobial screening

This method was important to test and display the inhibitory effect of synthesised compounds against the microorganism but not essential to kills it. The lowest concentration of an antimicrobial that was inhibit the visible growth of a microorganism and minimum bactericidal concentration as the lowest concentration that prevents the growth of an organism, from these we have to determine the level of activity of particular chemical compounds. For the synthesized complexes, two factors are applicable i.e. the ligands that are chelated to metal ions in a multidentate fashion, and nature of the ligand [18]. Complexes shows the diverse antibacterial activity, these may be the main reasons from these studies. The data reveals that all the complexes have higher antimicrobial activity than neutral bidentate ligands and a metal salt. Re(I) metal ions have ability to penetrate into bacterial cell and inactivate their enzymes, or can generate peroxy radical to kill bacteria these was also proven by lipid peroxidation and reactive oxygen spices. From Fig. 8, we observe that the antimicrobial screening of all complexes against different microorganisms is better than that of the respective ligands. The MIC values of the complexes, ligands, and metal salt are observed in the range of 40–80 µM, 275–330 µM, and > 2500 µM, respectively. Complexes (II) and (IV) is the most active amongst all the complexes and ligands, due to the presence of

the three metal carbonyl covalent bond, one chlorine directly attaced to metal ion, imidazole-pyrazoline ring substituents in the (2-butyl-5-chloro-1H-imidazol-4-yl)-4,5-dihydro-1H-pyrazole ligands. The increasing order of MIC value is **$Re(CO)_5Cl < L^1 = L^6 < L^3 < L^2 < L^4 < L^5 <$ I < VI < III < V < II < IV**. From these, it is increasingly important to determine the MIC in order to make the best choice in pharmaceuticals as antibiotics.

2.3.5 Reactive oxygen species (ROS)

Toxic nature of synthesised compounds further proved by reactive oxygen species and lipid peroxidation. In these study inorganic compounds having metal are capable of producing free radicals in biological system. The toxic effect of compounds on obstacle growth of saccharomyces cerevisiae were evaluated by quantification of H_2O_2, a reactive oxygen species. Here we found that cells treated with synthesised compounds having increasing amount i.e. 20–100 µg/mL were showing increased accumulation of H_2O_2 mmol/mL, as compared to untreated cells, here our synthesised compound having good reduction capability to produced free radicals. Compounds amount in microgram capable to produce peroxide in mmol concentration, these was positive point of these study. As the test sample concentration increase there was increase in H_2O_2 concentration. The decreasing order of H_2O_2 accumulation is: **I > VI > III > $L^1 \approx L^6$ > II > V ≈ IV > $L^3 > L^2 > L^5 > L^4$ > amphotericin-B > terbinafine > norfloxacine > ciprofloxacin** (Fig. 9). From the results, complexes show comparatively higher toxic effect than ligands and it means ROS depends on the metal concentration, functionality on compounds, which was further confirmed by observing their effects on DNA integrity of *Saccharomyces cerevisiae* as higher H_2O_2 causes for DNA damage.

2.3.6 Lipid Peroxidation

This study has linear relationship between reactive oxygen species. Increasing concentration of ROS can react with the unsaturated fatty acids of lipid membrane and stimulate lipid peroxidation. Reactive oxygen species randomly react with unsaturated fatty acid cause oxidative stress on *S. cerevices* and cause damage on yeast. Organic ligands (L^1-L^6) and inorganic metal complexes (I-VI) having ability to produce reactive oxygen species enhances the oxidative stress level. The lipid reaction resulted into formation of peroxide and degradation of fatty acid produced the MDA content. From the result the MDA content higher in complexes than the ligands mean toxic nature of complexes higher than the ligands, means complexes have higher capability to produce MDA concentration to kill the harmful cell. In future this method is very useful in the cancer treatment. The decreasing order of production of MDA is **IV > VI > III > $L^4 > L^6$ > II > I > V > $L^2 \approx L^3 > L^1 \approx L^5$ > amphotericin-B > terbinafine > norfloxacine > ciprofloxacin** (Fig. 10).

2.3.7 DNA interactions

Absorption titration

Binding of metal complexes with DNA via intercalation generally results in hypochromism and a red shift (bathochromism) of the absorption band [19]. The intercalation is due to a strong stacking interaction

between an aromatic moiety of the ligand and the base pair of the DNA [20, 21]. For rhenium(I) there was decrease in absorption (hypochromism) 1–2 nm and small red shift. The decreasing order of binding constant is: **IV > I > III > VI > V > L^3 > L^4 > L^5 > L^6 > L^1 > II > L^2**. It suggests that all synthesized complexes show groove binding, also confirmed by viscosity measurement and molecular docking. The organic anti-tumor drug netropsin has to bind within the DNA minor groove. The drug is held in place by amide hydrogen bonds to adenine N-3 and thymine O^{-2} atoms [22]. The binding mode and binding constant (K_b) of a complex toward DNA gives an idea about the strength of interaction, which can be obtained by studying UV-Vis. Complex bind to DNA through major or minor groove results in hypochromism and small red shift [22]. The binding constant (K_b) values estimated from the ratio of the intercept. The absorption spectral changes were monitored at around 276.0 -288.5 nm for the investigation of the DNA binding mode and strength (Fig. 11). As the DNA concentration was increased, the transition bands of the complexes (I-VI) exhibited hypochromicity [hypochromicity, H% = $[(A_{free} - A_{bound})/A_{free}] \times 100\%$] of about 3.32–24.7 %, and bathochromicity of 1-2.5 nm. The complex (IV) and the ligand (L^4) had the highest percentage of hypochromicity (IV- 18.45 %, L^4-24.7 %) (Table 2).

Table 2
Binding constant (K_b), percentage hypochromicity (%H), bathochromicity (Δλ), and Gibb's free energy (ΔG^0) values of free ligands and synthesized complexes

Compounds	λ_{max}		[a]Δλ(nm)	[b]K_b	[c]H%	[d]ΔG^0
	Bound	Free		$(M^{-1}) \times 10^6$		$(Jmol^{-1}{}^oK^{-1})$
L^1	265.5	268.5	3.0	2.0	25.7	-8590.9
L^2	267.5	270.5	3.0	0.6	10.7	-7878.0
L^3	272.5	276.5	4.0	3.0	9.30	-8831.0
L^4	270.5	275.5	5.0	2.8	24.7	-8790.1
L^5	271.5	275.0	3.5	2.3	10.9	-8673.7
L^6	273.5	279.5	6.5	2.2	9.63	-8647.3
I	288.5	290.5	2.0	4.3	13.2	-9044.2
II	287.0	288.5	1.5	1.7	13.4	-8494.7
III	276.0	278.5	2.5	4.2	6.07	-9030.2
IV	288.5	289.5	1.0	8.8	18.45	-9468.3
V	282.5	284.5	1.5	4.0	3.50	-9001.3
VI	282.5	284.0	1.5	4.1	3.32	-9016.0

[a]Δλ = Difference between bound wavelength and free wavelength.

[b]K_b = Intrinsic DNA binding constant determined from the UV–visible absorption spectral titration

[c]H% = $[(A_{free} - A_{bound})/A_{free}] \times 100\%$.

[d]ΔG^0 = Change in Gibb's free energy

2.3.8 Viscosity measurement

Viscosity measurements have been carried out on DNA by varying the concentration of the added Re(I) complex to get an idea of the binding mode. Groove binding typically causes less pronounced or only a minor change in the viscosity [23]. The values of relative specific viscosity $(\eta/\eta^0)^{1/3}$ [(η and η^0) are the specific viscosities] of DNA in the presence and absence of the Re(I)complex are plotted against [Re(I)complex]/[DNA] (Fig. 12). The ability to decrease the $(\eta/\eta^0)^{1/3}$ of DNA varies in the order is: **IV > VI > I > V > II > L^4 > L^6 > II > L^2 > L^1 > L^3 > L^5**, which parallels the DNA binding affinity. The increase in viscosity, observed in the presence of complex (I-VI) is small compared to the classical DNA intercalator EB [24].

The enhancement in viscosity observed in the presence study is also similar to minor groove binder netropsin [25]. These shows that complex I–VI, is more likely to have a DNA groove binding propensity [16, 25].

2.3.9 Molecular modelling with DNA sequence d(ACCGACGTCGGT)2

Molecular docking study is attempted to have an idea on the binding sites and favored orientation of the ligand and metal complex inside the DNA groove [26, 27]. The complexes and ligands are shown by ball and stick model and DNA base pair shown by VDW sphere using Hex 8.0 software. Structure of ligands and complexes drawn in .CDX format using ChemBioDraw Ultra 14.0 then converted to PDB format using Chem3D (Cambridge Soft). For docking studies the structural coordinates of HS-DNA was obtained from the protein data bank (pdb id: 423D) [28]. Figure 13 shows that Re(I) complexes binds with the base pair A–T, C–G, G–C, A–T (B-DNA) minor grooves of the DNA. The increasing order of energy is: **L^6 < L^2 < L^4 < L^1 < L^5 < VI < II < IV < I < V < L^3 < III**. Docking image and docking energy are summarized in supplementary material 2.

2.3.10 Effect of compounds on the integrity of S. cerevisiae cells

Agarose gel electrophoresis is a convenient method to assess the cleavage of DNA by metal based drugs [29], to determine the factors affecting the nucleolytic efficiency of a compound and to compare the nucleolytic properties of different compounds. The DNA damaging potentiality of the compounds gives a characteristic picture of comets was observed when DNA were unveiled to increasing concentrations of compounds and increasing in smearing was observed. The electrophoretic separation of DNA when reacted with compounds under aerobic conditions, they first bound to the DNA, when electric field was applied DNA and RNA fragment by length occurs thorough showing comets like smearing observed. These clearly shows that the relative binding efficacy of the complexes to DNA is much higher than the binding efficacy of imidazole-pyrazoline heterocyclic ligands. The difference in the DNA-cleavage efficiency of the complexes and ligands is due to the difference in binding affinity of the ligands and complexes to the DNA. In Fig. 14 ligands shows lesser smearing as compared to the complexes at 24 h time interval after at 48 h treatment DNA with complexes was completely degraded. It suggests that the cleavage efficiency of DNA is higher in complexes than the ligands. All complexes (I-VI) show better cleavage efficacy to DNA, and ligands (L^1-L^6) show lesser cleavage effect to DNA.

3. Conclusions

A series of bis heterocycles imidazole-pyrazoline nucleus based organometallic rhenium(I) complexes were synthesized and well characterized, in search of new organometallic complexes show better antibacterial, cytotoxicity, reactive oxygen species, lipid peroxidation, genotoxicity, DNA binding and DNA

cleavage study. Treatment of Re(I) compounds was causes changes in DNA and genotoxicity using *Saccharomyces cerevisiae* yeast. From the result of genotoxicity we have to acquire higher H_2O_2 production in complexes as compared to ligands these result comparable to lipid peroxidation. The new synthetic approach was carried out by penta carbonyl chloro rhenium(I) as starting material for preparing the novel organometallic complexes having octahedral structure and non-electrolytic nature. DNA binding study proved by absorption titration, viscosity measurement and molecular modelling. Binding constant (K_b) values of complexes higher than the ligands, it shows higher binding capability of complexes with DNA i.e. groove binding. Viscosity in presence and absence of Re(I) complex there was negligible change in time of about 1–3 millisecond, it suggest groove binding means there was minor DNA lengthening observed. In molecular modelling docking energy of complexes higher than the ligands. The presence of a carbon monoxide directly attached with Re(I) metal ion and imidazole-pyrimidine nucleus chelated with rhenium(I) metal improves biological activity. Complexes (I-VI) having higher IC_{50} value than cisplatin, carboplatin, oxaliplatin. All the complexes show good vitro cytotoxic, cellular level bioassay, reactive oxygen species, and lipid peroxidation compared to free ligands.

4. Experimental

4.1 Materials and methods

All the chemicals and solvents were of the reagent grade. 2-Acetyl thiophene and substituted aldehydes were purchased from Merck Limited (India). Substituted phenyl hydrazines were purchased from Thirumalai Chemicals Ltd. (TCL). Potassium-tert-butoxide, potassium hydroxide was purchased from Sisco Research Laboratories Pvt. Ltd. (SRL). Penta carbonyl chloro rhenium(I) was purchased from Sigma Aldrich (USA). Luria broth, agarose and nutrient broth were purchased from Himedia (India). The culture of two Gram(+ ve), i.e. *Staphylococcus aureus* (*S. aureus*) (MTCC-3160) and *Bacillus subtilis* (MTCC-7193), and three Gram(-ve), i.e. *Serratia marcescens* (MTCC-7103), *Pseudomonas aeruginosa* (MTCC-1688) and *Escherichia coli* (MTCC-433), were purchased from Institute of Microbial Technology (Chandigarh, India). *S. cerevisiae* Var. Paul Linder 3360 was obtained from IMTECH, Chandigarh, India. HS DNA was purchased from Sigma Aldrich Chemical Co. (India). Human colorectal carcinoma (HCT 116) cells were obtained from the cell repository, National Center for Cell Science (NCCS), Pune, Maharashtra, India.

4.2 Instrumentation

The ^{1}H and ^{13}C NMR spectra were recorded on a Bruker Avance (400 MHz). Infrared spectra were recorded on an FT–IR ABB Bomen MB 3000 spectrophotometer in the range 4000–400 cm^{-1}. C, H, and N elemental analyses were performed with a Heraeus, Germany CHNO RAPID. Molar conductance was measured using conductivity meter model no. EQ-660A, Mumbai (India). Melting points (°C, uncorrected) were determined in open capillaries on ThermoCal10 melting point apparatus (Analab Scientific Pvt. Ltd, India).The electronic spectra were recorded on a UV–160A UV–Vis spectrophotometer, Shimadzu (Japan). The minimum inhibitory concentration (MIC) study was carried out by means of laminar air flow

cabinet (Toshiba, Delhi, India). Hydrodynamic chain length study was carried out by viscometric measurement bath. Photo quantization of the gel after electrophoresis was carried out on AlphaDigiDocTM RT. Version V.4.0.0 PC–Image software.

4.3 General method for synthesis of 1,3,5- trisubstituted pyrazole ligands (L^1-L^6)

The α,β unsaturated carbonyl compounds (3a-3f) have been synthesized using literature procedure [30]. Synthesis of the trisubstituted pyrazoline based ligands (L^1-L^6) have been carried out. To a solution of α, β unsaturated carbonyl compounds (3a-3f) (2.95 mmol) in 10 mL of ethanol, substituted phenyl hydrazine (4a-4f) (0.245 g, 2.95 mmol) and K^tOBu (0.25 g, 0.1 mmol) solution were added. The reaction mixture was refluxed for 4 hr. Completion of reaction checked by TLC plates, the excess of solvent was removed under reduced pressure and the reaction mixture was cooled on an ice bath. The resulting mixture was concentrated under vacuum to obtain the bis heterocyclic ligands as a product. The general reaction scheme for the synthesis of ligands (L^1-L^6) shows in Fig. 2. The ^1H and ^{13}C NMR spectra are shown in supplementary material 1.

4.3.1 5-(2-Butyl-5-chloro-1H-imidazol-4-yl)-1,3-diphenyl-4,5-dihydro-1H-pyrazole (L^1)

This ligand (L^1) has prepared through the addition of α,β-unsaturated enone (3a) (408 mg, 1.479 mmol) and phenyl hydrazine (123 mg, 1.479 mmol), after 5–6 h reflux; Yield: 70%; Color: yellowish crystalline solid; **m.p.**: 172°C; **Mol. wt.**: 378.90 g/mol; **Empirical formula**: $C_{22}H_{23}ClN_4$, **Elemental analysis**: Calc. (%):C, 69.74; H, 6.12; N, 14.79; found(%).C, 69.66; H, 6.02; N, 14.71; **Mass spectra (m/z %)**: 378.86 (100) [M^+], 380.86 [M + 2]; **^1H NMR (400 MHz, DMSO-d_6) δ/ppm**: 12.10 (1H, s, -NH), 7.56 (2H, d, J = 8.8 Hz, H4”,4'"), 7.38 (2H, d, J = 8.4 Hz, H2",6"), 7.23 (2H, d, J = 4.4 Hz, H3",5"), 7.04 (2H, d, J = 4.0 Hz, H3'",5'"), 6.84 (2H, d, J = 8.8 Hz, H2",6"), 5.16 (1H, dd, J1 = 4.0, J2 = 8.4, H3), 3.80 (1H, dd, J1 = 9.2 Hz, J2 = 10.0, H4b), 2.94 (1H, dd, J1 = 10.0, J2 = 12.0, H4a), 1.45 (2H, m, H2'a), 1.21 (2H, m, H2'b), 0.82 (2H, m, H2'c), 0.73 (3H, m, -H2'd). **^{13}C NMR (100 MHz, DMSO-d_6) δ/ppm**: 151.0 (C5, Cquat.),147.6 (C2', Cquat.), 142.9 (C1'", Cquat.), 138.1 (C1", Cquat.), 135.9 (C5', Cquat.), 125.1 (C4', Cquat.), 126.6 (C4”, -CH), 124.5 (C3",5", -CH),123.1 (C2",C6", −CH), 118.9 (C4'", −CH), 116.1 (C3'",5'", −CH), 113.9 (C2'",6'", −CH), 54.7 (C3, −CH), 29.9 (C4, $-CH_2$), 27.1 (C2'a, $-CH_2$), 26.9 (C2'b, $-CH_2$), 21.0 (C2'c, $-CH_2$),13.8(C2'd, $-CH_3$). [**Total signal observed** = 18: signal of C = 06 (phenyl ring-C = 2, pyrazoline = 1, imidazole ring-C = 3), signal of -CH = 07 (pyrazoline -CH = 1, phenylring -CH = 6), signal of $-CH_2$ = 04 (pyrazoline $-CH_2$ = 1, imidazole $-CH_2$ = 3), $-CH_3$ = 1]. **IR spectra** (KBr, 4000–400 cm^{-1}): 3253 ν(-NH)stret., 2906 ν(-CH)stret. alkane, 2844 ν(= CH)stret., 2320 ν(-C-N)stret., 1564, 1463 ν(C = N), 1209 ν(C = C)stret., 1062, 800 ν(para substitution), 615, 592 ν(C-Cl).

4.3.2 5-(2-Butyl-5-chloro-1H-imidazol-4-yl)-1,3-bis(4-chlorophenyl)-4,5-dihydro-1H-pyrazole (L^2)

This ligand (L^2) has prepared through the addition of α,β-unsaturated enone (3b) (408 mg, 1.479 mmol) and 4- Cl phenyl hydrazine (123 mg, 1.479 mmol), after 5–6 h reflux; Yield: 72%; Color: yellowish crystalline solid; **m.p.**: 182°C; **Mol. wt.**: 447.79 g/mol; **Empirical formula**: $C_{22}H_{21}Cl_3N_4$; **Elemental analysis**: Calc. (%);C, 59.01; H, 4.73; N, 12.51; found(%). C, 58.96; H, 4.64; N, 12.46; **Mass spectra (m/z %)**: 447.74 (100) [M^+], 449.74 [M + 2], 451.74 [M + 4], 453.73 [M + 6]. **^{1}H NMR (400 MHz, DMSO-d_6) δ/ppm**: 12.31 (1H, s, -NH), 7.78 (2H, d, J = 8.8 Hz, H2",6"), 7.52 (2H, d, J = 8.8 Hz, H3",5"), 7.25 (2H, d, J = 8.4 Hz, H3‴,5‴), 7.04 (2H, d, J = 8.4 Hz, H2‴,6‴), 5.37 (1H, dd, J1 = 8.4, J2 = 4.0, H3), 3.87 (1H, dd, J1 = 7.2 Hz, J2 = 12.8, H4b), 3.24 (1H, dd, J1 = 8.0, J2 = 9.6, H4a), 1.56 (2H, m, H2'a), 1.20 (2H, m, H2'b), 0.97 (2H, m, H2'c), 0.90 (3H, m, -H2'd). **^{13}C NMR (100 MHz, DMSO-d_6) δ/ppm**: 148.4 (C5, Cquat.),147.8 (C2', Cquat.), 143.7 (C1‴, Cquat.), 138.8 (C4", Cquat.), 137.7 (C1", Cquat.), 133.8 (C4‴, Cquat.), 131.4 (C5', Cquat.), 130.3 (C3‴,5‴, -CH), 129.5 (C3",C5", −CH), 128.3 (C2",6", −CH), 123.4 (C4', Cquat.), 115.0 (C2‴,6‴, −CH), 55.2 (C3, −CH), 30.1 (C4, $-CH_2$), 28.3 (C2'a, $-CH_2$), 27.9 (C2'b, $-CH_2$), 22.1 (C2'c, $-CH_2$), 14.0 (C2'd, $-CH_3$). [**Total signal observed** = 18: signal of C = 08 (phenyl ring-C = 4, pyrazoline = 1, imidazole ring-C = 3), signal of -CH = 05 (pyrazoline -CH = 1, phenylring -CH = 4), signal of $-CH_2$ = 04 (pyrazoline $-CH_2$ = 1, imidazole $-CH_2$ = 3), $-CH_3$ = 1]. **IR Spectra** (KBr, 4000–400 cm^{-1}): 3252 ν(-NH)stret., 2934 ν(-CH)stret. alkane, 2819 ν(= CH)stret., 2332 ν(-C-N)stret., 1576, 1468 ν(C = N), 1222 ν(C = C)stret., 1067, 805 ν(para substitution), 620, 558 ν(C-Cl).

4.3.3 5-(2-Butyl-5-chloro-1H-imidazol-4-yl)-1,3-di-p-tolyl-4,5-dihydro-1H-pyrazole (L^3)

This ligand (L^3) has prepared through the addition of α,β-unsaturated enone (3c) (408 mg, 1.479 mmol) and 4-CH_3 phenyl hydrazine (123 mg, 1.479 mmol), after 5–6 h reflux; Yield: 74%; Color: yellowish crystalline solid; **m.p.**: 169°C; **Mol. wt.**: 406.96 g/mol; **Empirical formula**: $C_{24}H_{27}ClN_4$, **Elemental analysis**: Calc. (%):C, 70.83; H, 6.69; N, 13.77; found(%).C, 70.78; H, 6.65; N, 13.64; **Mass spectra (m/z %)**: 406.87 (100) [M^+], 408.87 [M + 2]; **^{1}H NMR (400 MHz, DMSO-d_6) δ/ppm**: 12.20 (1H, s, -NH), 7.71 (2H, d, J = 8.4 Hz, H3",5"), 7.47 (2H, d, J = 10.8 Hz, H2",6"), 7.36 (2H, d, J = 8.8 Hz, H2‴,6‴), 6.98 (2H, d, J = 8.8 Hz, H3‴,5‴), 5.37 (1H, dd, J1 = 4.0, J2 = 9.2, H3), 3.88 (1H, dd, J1 = 5.6 Hz, J2 = 9.2, H4b), 3.22 (1H, dd, J1 = 8.0, J2 = 9.6, H4a), 2.48 (6H, s, 2-CH_3), 1.63 (2H, m, H2'a), 1.35 (2H, m, H2'b), 0.96 (2H, m, H2'c), 0.85 (3H, m, -H2'd). **^{13}C NMR (100 MHz, DMSO-d_6) δ/ppm**: 148.9 (C5, Cquat.), 148.3 (C2', Cquat.), 144.1 (C4", Cquat.), 143.5 (C1‴, Cquat.), 139.0 (C1", Cquat.), 136.0 (C4‴, Cquat.), 133.3 (C5', Cquat.), 129.1 (C3‴,5‴, -CH), 128.5 (C3",C5", −CH), 125.9 (C2",6", −CH), 123.0 (C4', Cquat.), 114.9 (C2‴,6‴, −CH), 55.0 (C3, −CH), 30.2 (C4, $-CH_2$), 28.9 (C2'a, $-CH_2$), 28.0 (C2'b, $-CH_2$), 22.0 (C2'c, $-CH_2$), 21.62 ($-CH_3$), 21.45 ($-CH_3$), 14.0 (C2'd, $-CH_3$). [**Total signal observed** = 20: signal of C = 08 (phenyl ring-C = 4, pyrazoline = 1, imidazole ring-C = 3), signal of -CH = 05 (pyrazoline -CH = 1, phenylring -CH = 4), signal of $-CH_2$ = 04 (pyrazoline $-CH_2$ = 1, imidazole $-CH_2$ = 3), $-CH_3$ = 3]. **IR Spectra**(KBr, 4000–400 cm^{-1}): 3252 ν(-NH)stret., 2912 ν(-CH)stret. alkane, 2843 ν(= CH)stret., 2334 ν(-C-N)stret., 1516, 1485 ν(C = N), 1215 ν(C = C)stret., 999, 798 ν(para substitution), 590, 544 ν(C-Cl).

4.3.4 5-(2-Butyl-5-chloro-1H-imidazol-4-yl)-1,3-bis(4-nitrophenyl)-4,5-dihydro-1H-pyrazole (L^4)

This ligand (L^4) has prepared through the addition of α,β-unsaturated enone (3d) (408 mg, 1.479 mmol) and 4-NO_2 phenyl hydrazine (123 mg, 1.479 mmol), after 5–6 h reflux; Yield: 80%; Color: yellowish crystalline solid; **m.p.**: 194°C; **Mol. wt.**: 468.90 g/mol; **Empirical formula**: $C_{22}H_{21}ClN_6O_4$, **Elemental analysis**: Calc.(%): C, 56.35; H, 4.51; N, 17.92; found(%).C, 56.29; H, 4.45; N, 18.04; **Mass spectra (m/z %)**: 468.84 (100) [M^+], 470.84 [M + 2]; **^{1}H NMR (400 MHz, DMSO-d_6) δ/ppm**: 12.37 (1H, s, -NH), 7.73 (2H, d, J = 3.6 Hz, H3",5"), 7.69 (2H, d, J = 12.0 Hz, H2",6"), 7.43 (2H, d, J = 11.2 Hz, H3‴,5‴), 7.16 (2H, d, J = 8.4 Hz, H2‴,6‴), 6.26 (1H, dd, J1 = 4.8, J2 = 6.8, H3), 4.01 (1H, dd, J1 = 4.8 Hz, J2 = 9.8, H4b), 3.24 (1H, dd, J1 = 5.2, J2 = 12.0, H4a), 1.68 (2H, m, H2'a), 1.35 (2H, m, H2'b), 0.92 (2H, m, H2'c), 0.85 (3H, m, H2'd). **^{13}C NMR (100 MHz, DMSO-d_6) δ/ppm**: 152.2 (C5, Cquat.), 148.4 (C1‴, Cquat.), 147.9 (C1", Cquat.), 144.0 (C2', Cquat.), 132.1 (C4", Cquat.), 132.4 (C2",6", -CH), 130.4 (C3",5", -CH), 127.1 (C3‴,5‴, -CH), 123.0 (C4‴, Cquat.), 122.5 (C5', Cquat.), 115.5 (C2‴,6‴, -CH), 111.1 (C4', −Cquat.), 55.0 (C3, −CH), 30.2 (C4, $-CH_2$), 28.4 (C2'a, $-CH_2$), 27.9 (C2'b, $-CH_2$), 22.1 (C2'c, $-CH_2$), 14.1 (C2'd, $-CH_3$). [**Total signal observed** = 18: signal of C = 08 (phenyl ring-C = 4, pyrazoline = 1, imidazole ring-C = 3), signal of -CH = 05 (pyrazoline -CH = 1, phenyl ring -CH = 4), signal of $-CH_2$ = 04 (pyrazoline $-CH_2$ = 1, imidazole $-CH_2$ = 3), $-CH_3$ = 1]. **IR Spectra** (KBr, 4000–400 cm^{-1}): 3259 ν(-NH)stret., 2931 ν(-CH)stret. alkane, 2846 ν(= CH)stret., 2337 ν(-C-N)stret., 1566, 1465 ν(C = N), 1226 ν(C = C)stret., 1049, 987 ν(para substitution), 617, 547 ν(C-Cl).

4.3.5 1,3-bis(4-Bromophenyl)-5-(2-butyl-5-chloro-1H-imidazol-4-yl)-4,5-dihydro-1H-pyrazole (L^5)

This ligand (L^5) has prepared through the addition of α,β-unsaturated enone (3e) (408 mg, 1.479 mmol) and 4-bromo phenyl hydrazine (123 mg, 1.479 mmol), after 5–6 h reflux; Yield: 60%; Color: yellowish crystalline solid; **m.p.**: 180°C; **Mol. wt.**: 536.70 g/mol; **Empirical formula**: $C_{22}H_{21}Br_2ClN_4$, **Elemental analysis**: Calc.(%): C, 49.23; H, 3.94; N, 10.44; found(%). C, 49.16; H, 3.88; N, 10.38; **Mass spectra (m/z %)**: 536.68 (100) [M+], 538.68 [M + 2], 540.68 [M + 4], 542.68 [M + 6]; **^{1}H NMR (400 MHz, DMSO-d_6) δ/ppm**: 12.30 (1H, s, -NH), 7.65 (2H, d, J = 11.6 Hz, H2",6"), 7.55 (2H, d, J = 9.2 Hz, H2",6"), 7.44 (2H, d, J = 11.2 Hz, H2‴,6‴), 7.14 (2H, d, J = 8.0 Hz, H3‴,5‴), 5.37 (1H, dd, J1 = 5.2, J2 = 8.4, H3), 4.09 (1H, dd, J1 = 6.8 Hz, J2 = 7.6, H4b), 3.84 (1H, dd, J1 = 7.6, J2 = 11.2, H4a), 1.67 (2H, m, H2'a), 1.33 (2H, m, H2'b), 0.96 (2H, m, H2'c), 0.92 (3H, m, H2'd). **^{13}C NMR (100 MHz, DMSO-d_6) δ/ppm**: 148.4 (C5, Cquat.),147.8 (C2', Cquat.), 143.7 (C1‴, Cquat.), 133.8 (C1", Cquat.), 131.4 (C5', Cquat.), 130.4 (C4", Cquat.), 129.8 (C3‴,5‴, -CH), 129.1 (C3",5", -CH), 127.9 (C2",6", -CH), 125.1 (C4', Cquat.), 123.4 (C4‴, Cquat.), 115.0 (C2‴,6‴, CH), 55.1 (C3, −CH), 30.2 (C4, $-CH_2$), 28.2 (C2'a, $-CH_2$), 27.9 (C2'b, $-CH_2$), 22.0 (C2'c, $-CH_2$), 14.0 (C2'd, $-CH_3$). [**Total signal observed** = 18: signal of C = 08 (phenyl ring-C = 4, pyrazoline = 1, imidazole ring-C = 3), signal of -CH = 05 (pyrazoline -CH = 1, phenyl ring -CH = 4), signal of $-CH_2$ = 04 (pyrazoline $-CH_2$ = 1, imidazole $-CH_2$ = 3), $-CH_3$ = 1]. **IR Spectra** (KBr, 4000–400 cm^{-1}): 3259 ν(-NH)stret., 2981 ν(-CH)stret. alkane, 2842 ν(= CH)stret., 2333 ν(-C-N)stret., 1569, 1485 ν(C = N), 1212 ν(C = C)stret., 798, 999 ν(para substitution), 590, 551 ν(C-Cl).

4.3.6 5-(2-Butyl-5-chloro-1H-imidazol-4-yl)-3-(3,4-dimethoxyphenyl)-1-(4-methoxyphenyl)- 4,5-dihydro-1H-pyrazole (L^6)

This ligand (L^6) has prepared through the addition of α,β-unsaturated enone (3f) (408 mg, 1.479 mmol) and 4-OCH_3 phenyl hydrazine (123 mg, 1.479 mmol), after 5–6 h reflux; Yield: 85%; Color: yellowish crystalline solid; **m.p.**: 178°C; **Mol. wt.**: 468.98 g/mol; **Empirical formula**: $C_{25}H_{29}ClN_4O_3$, **Elemental analysis**: Calc. (%):C, 64.03; H, 6.23; N, 11.95; found. C, 63.94; H, 6.16; N, 11.88; **Mass spectra (m/z %)**: 468.95 (100) [M+];470.95 [M + 2]; **^{1}H NMR (400 MHz, DMSO-d_6) δ/ppm**: 12.18 (1H, s, -NH), 7.74 (1H, d, J = 8.0 Hz, H6''), 7.68 (1H, d, J = 11.2 Hz, H2''), 7.44 (1H, d, J = 11.2 Hz, H5''), 7.14 (2H, d, J = 5.6 Hz, H2''',6'''), 7.05 (2H, d, J = 8.0 Hz, H3''',5'''), 5.16 (1H, dd, J1 = 4.0, J2 = 8.4, H3), 3.96 (9H, s, 3-OCH_3), 3.65 (1H, dd, J1 = 4.8 Hz, J2 = 12.4, H4b), 3.13 (1H, dd, J1 = 8.0, J2 = 11.2, H4a), 1.69 (2H, m, H2'a), 1.34 (2H, m, H2'b), 0.97 (2H, m, H2'c), 0.91 (3H, m, H2'd). **^{13}C NMR (100 MHz, DMSO-d_6) δ/ppm**: 153.6 (C5, Cquat.), 151.7 (C4''', Cquat.), 149.3 (C4'', Cquat.), 141.1 (C3'', Cquat.), 139.7 (C2', Cquat.), 128.6 (C1''', Cquat.), 127.1 (C1'', Cquat.),126.1 (C5', Cquat.), 126.5 (C6'', -CH), 123.1 (C2'', -CH), 123.1 (C4', Cquat.), 117.9 (C5'', –CH), 111.0 (C3''',5''', -CH), 110.6 (C2''',6''', -CH), 56.2 (-OCH_3), 56.0 (-OCH_3), 55.8 (-OCH_3), 55.45 (C3, -CH), 30.7 (C4, –CH_2), 30.0 (C2'a, –CH_2), 28.3 (C2'b, -CH_2), 22.1 (C2'c, -CH_2), 14.0 (C2'd, -CH_3). [**Total signal observed** = 23: signal of C = 09 (phenyl ring-C = 3, pyrazoline = 1, imidazole ring-C = 3), signal of -CH = 06 (pyrazoline -CH = 1, phenylring -CH = 5), signal of –CH_2 = 04 (pyrazoline –CH_2 = 1, imidazole –CH_2 = 3), -CH_3 = 1, -OCH_3 = 3]. **IR Spectra** (KBr, 4000–400 cm^{-1}): 3259 ν(-NH)stret., 3005 ν(-CH)stret. alkane, 2843 ν(= CH)stret., 2334 ν(-C-N)stret., 1516, 1485 ν(C = N), 1215 ν(C = C)stret., 999 ν(para substitution), 590, 630 ν(C-Cl).

4.4 General method for synthesis of -N,N donor complexes (I-VI)

Ethanolic solution of the precursor of [$Re(CO)_5Cl$] (0.220 g, 0.8 mmol) was refluxed for 10 minutes. Then a solution of ligand (L^1-L^6) (0.300 g, 0.6 mmol in 10mL ethanol), was added and the reaction was stirred yielding a brownish red solution. The resulting mixture was stirred at 70-90°C temperature for 8–10 h. the progress of reaction was monitored by TLC after completion of reaction the solution was filtered through celite in order to remove solid particles and the solvent was removed under reduced pressure the brown crystalline product was obtained. The proposed reaction scheme for the synthesis of complexes (I-VI) is shown in Fig. 3.

4.4.1 Synthesis of [$Re(CO)_3(L^1)Cl$] (I)

It was synthesized using ligand (**L^1**) (0.316 g, 1.0 mmol).Yield: 80%; Color: brown crystalline solid; **m.p.**: 378°C; **Mol. wt.**: 684.59 g/mol; **Empirical formula**: $C_{25}H_{23}Cl_2N_4O_3Re$, **Elemental analysis**: **Calc. (%)**: C, 43.86; H, 3.39; N, 8.18; Re, 27.20; **Found (%)**:C, 43.83; H, 3.36; N, 8.16; Re, 27.16; **Conductance**: 2.10 ohm^-

$^{1}cm^{2}mol^{-1}$; **^{1}H NMR (400 MHz, DMSO-d_6) δ/ppm**: 12.17 (1H, s, -NH), 7.74 (2H, d, J = 4.8 Hz, H4",4'"), 7.58 (2H, d, J = 8.4 Hz, H2",6"), 7.54 (2H, d, J = 4.8 Hz, H3",5"), 7.24 (2H, d, J = 4.0 Hz, H3'",5'"), 6.94 (2H, d, J = 8.8 Hz, H2",6"), 5.28 (1H, dd, J1 = 4.4, J2 = 10.4, H3), 3.81 (1H, dd, J1 = 7.2 Hz, J2 = 9.2, H4b), 3.13 (1H, dd, J1 = 8.0, J2 = 9.6, H4a), 1.46 (2H, m, H2'a), 1.11 (2H, m, H2'b), 0.90 (2H, m, H2'c), 0.83 (3H, m, H2'd). **^{13}C NMR (100 MHz, DMSO-d_6) δ/ppm**: 188.08 (2M-CO, Cquat.), 186.78 (M-CO, Cquat.), 151.9 (C5, Cquat.), 148.9 (C2', Cquat.), 143.9 (C1'", Cquat.), 139.1 (C1", Cquat.), 135.6 (C5', Cquat.), 125.0 (C4', Cquat.), 127.6 (C4", -CH),123.5 (C3",5", -CH), 123.1 (C2",C6", −CH), 119.9 (C4'", −CH), 118.2 (C3'",5'", −CH), 114.9 (C2'",6'", −CH), 55.0 (C3, −CH), 30.0 (C4, $-CH_2$), 28.2 (C2'a, $-CH_2$), 27.9 (C2'b, $-CH_2$), 21.3 (C2'c, $-CH_2$) 14.0 (C2'd, $-CH_3$). [**Total signal observed** = 20: signal of C = 08 (M-CO = 2, phenyl ring-C = 2, pyrazoline = 1, imidazole ring-C = 3), signal of -CH = 07 (pyrazoline -CH = 1, phenylring -CH = 6), signal of $-CH_2$ = 04 (pyrazoline $-CH_2$ = 1, imidazole $-CH_2$ = 3), $-CH_3$ = 1]. **IR spectra** (KBr, 4000–400 cm^{-1}): 3310 ν(-NH)stret.,2954 ν(-CH)stret. alkane,2931 ν(= CH)stret.,2345 ν(-C-N)stret.,1882, 2021 ν(M-CO), 1589, 1488 ν(C = N),1311 ν(C = C)stret., 825 ν(para substitution)617,640 ν(C-Cl),570 ν(Re-N).

4.4.2 Synthesis of [Re(CO)$_3$(L^2)Cl] (II)

It was synthesized using ligand (**L^2**) (0.316 g, 1.0 mmol). Yield: 84%; Color: brown crystalline solid; **m.p.**: 382°C; **Mol. wt.**: 753.48 g/mol; **Empirical formula**: $C_{25}H_{21}Cl_4N_4O_3Re$. **Elemental analysis**: **Calc. (%)**:C, 39.85; H, 2.81; N, 7.44; Re, 24.71; **Found (%)**:C, 39.82; H, 2.78; N, 7.42; Re, 24.69; **Conductance**: 4.50 $ohm^{-1}cm^{2}mol^{-1}$; **^{1}H NMR (400 MHz, DMSO-d_6) δ/ppm**: 12.30 (1H, s, -NH), 7.78 (2H, d, J = 8.4 Hz, H2",6"), 7.52 (2H, d, J = 8.4 Hz, H3",5"), 7.25 (2H, d, J = 8.8 Hz, H3'",5'"), 7.04 (2H, d, J = 8.8 Hz, H2'",6'"), 5.37 (1H, dd, J1 = 8.4, J2 = 11.6, H3), 3.88 (1H, dd, J1 = 6.0 Hz, J2 = 10.8, H4b), 3.23 (1H, dd, J1 = 7.6, J2 = 9.6, H4a), 1.54 (2H, m, H2'a), 1.21 (2H, m, H2'b), 0.89 (2H, m, H2'c), 0.83 (3H, m, H2'd). **^{13}C NMR (100 MHz, DMSO-d_6) δ/ppm**: 196.8 (2M-CO, Cquat.), 188.6 (M-CO, Cquat.), 152.0 (C5, Cquat.), 151.3 (C2', Cquat.), 137.3 (C1'", Cquat.), 133.9 (C3'",5'", -CH), 133.5 (C4", Cquat.), 129.9 (C1", Cquat.), 129.3 (C4'", Cquat.), 129.2 (C5', Cquat.), 128.6 (C4', Cquat.), 125.8 (C3",5", −CH), 123.6 (C2",6", -CH), 117.9 (C2'",6'", −CH), 55.1 (C3, −CH), 30.0 (C4, $-CH_2$), 28.3 (C2'a, $-CH_2$), 27.9 (C2'b, $-CH_2$), 22.1 (C2'c, $-CH_2$), 14.1 (C2'd, $-CH_3$). [**Total signal observed** = 20: signal of C = 10 (M-CO = 2, phenyl ring-C = 4, pyrazoline = 1, imidazole ring-C = 3), signal of -CH = 05 (pyrazoline -CH = 1, phenylring -CH = 4), signal of $-CH_2$ = 04 (pyrazoline $-CH_2$ = 1, imidazole $-CH_2$ = 3), $-CH_3$ = 1]. **IR spectra** (KBr, 4000–400 cm^{-1}): 3278 ν(-NH)stret., 2954 ν(-CH)stret. alkane, 2839 ν(= CH)stret., 2352 ν(-C-N)stret., 1890, 2013 ν(M-CO), 1596, 1488 ν(C = N), 1319 ν(C = C)stret., 1018, 825 ν(para substitution), 640 ν(C-Cl), 578 ν(Re-N).

4.4.3 Synthesis of [Re(CO)$_3$(L^3)Cl] (III)

It was synthesized using ligand (**L^3**) (0.316 g, 1.0 mmol). Yield: 76%; Color: brown crystalline solid; **m.p.**: 372°C; **Mol. wt.**: 712.65 g/mol; **Empirical formula**: $C_{27}H_{27}Cl_2N_4O_3Re$, **Elemental analysis**: **Calc. (%)**:C, 45.51; H, 3.82; N, 7.86; Re, 26.13; **Found (%)**:C, 45.48; H, 3.82; N, 7.83; Re, 26.10; **Conductance**: 6.78 $ohm^{-1}cm^{2}mol^{-1}$; **^{1}H NMR (400 MHz, DMSO-d_6) δ/ppm**: 12.23 (1H, s, -NH), 8.03 (2H, d, J = 6.8 Hz, H3",5"), 7.68

(2H, d, J = 6.8 Hz, H2",6"), 7.48 (2H, d, J = 7.6 Hz, H2'",6'"), 7.21 (2H, d, J = 11.6 Hz, H3'",5'"), 5.76 (1H, dd, J1 = 5.2, J2 = 10.4, H3), 4.20 (1H, dd, J1 = 5.6 Hz, J2 = 11.2, H4b), 3.41 (1H, dd, J1 = 6.8, J2 = 11.2, H4a), 2.34 (6H, s, 2-CH_3), 1.61 (2H, m, H2'a), 1.31 (2H, m, H2'b), 0.89 (2H, m, H2'c), 0.74 (3H, m, -H2'd). **^{13}C NMR (100 MHz, DMSO-d_6) δ/ppm**: 189.28 (2M-CO, Cquat.), 188.08 (M-CO, Cquat.), 151.9 (C5, Cquat.),148.9 (C2', Cquat.), 148.3 (C4", Cquat.), 144.1 (C1'", Cquat.), 143.9 (C1", Cquat.), 139.1 (C4'", Cquat.), 125.9 (C5', Cquat), 123.5 (C4', Cquat.), 135.6 (C3'",5'", -CH), 128.3 (C3",5", -CH), 126.3 (C2",C6", −CH), 114.9 (C2'",6'", −CH), 55.0 (C3, −CH), 30.1 (C4, −CH_2), 28.2 (C2'a, −CH_2), 27.9 (C2'b, -CH_2), 22.0 (C2'c, -CH_2), 21.6 (-CH_3), 20.3 (-CH_3), 14.1 (C2'd, -CH_3). [**Total signal observed** = 22: signal of C = 10 (M-CO = 2, phenyl ring-C = 4, pyrazoline = 1, imidazole ring-C = 3), signal of -CH = 05 (pyrazoline -CH = 1, phenylring -CH = 4), signal of −CH_2 = 04 (pyrazoline −CH_2 = 1, imidazole −CH_2 = 3), -CH_3 = 3]. **IR Spectra** (KBr, 4000–400 cm^{-1}): 3278 ν(-NH)stret., 2931 ν(-CH)stret. alkane, 2862 ν(= CH)stret., 2360 ν(-C-N)stret., 1890, 2013 ν(M-CO), 1512, 1458 ν(C = N), 1249 ν(C = C)stret., 1026, 825 ν(para substitution), 617, 640 ν(C-Cl), 570 ν(Re-N).

4.4.4 Synthesis of [Re(CO)$_3$(L^4)Cl] (IV)

It was synthesized using ligand (**L^4**) (0.316 g, 1.0 mmol). Yield: 78%; Color: brown crystalline solid; **m.p.**: 390°C; **Mol. wt.**: 774.59 g/mol; **Empirical formula**: $C_{25}H_{21}Cl_2N_6O_7Re$, **Elemental analysis**: **Calc. (%)**: C, 38.77; H, 2.73; N, 10.85; Re, 24.04; **Found (%)**: C, 38.75; H, 2.69; N, 10.82; Re, 24.00; **Conductance**: 3.18 $ohm^{-1}cm^2mol^{-}1$; **^{1}H NMR (400 MHz, DMSO-d_6) δ/ppm**: 12.41 (1H, s, -NH), 7.92 (2H, d, J = 8.0 Hz, H3",5"), 7.64 (2H, d, J = 8.8 Hz, H2",6"), 7.36 (2H, d, J = 7.6 Hz, H3'",5'"), 7.26 (2H, d, J = 8.0 Hz, H2'",6'"), 5.31 (1H, dd, J1 = 5.6, J2 = 10.8, H3), 3.85 (1H, dd, J1 = 7.2 Hz, J2 = 11.2, H4b), 3.20 (1H, dd, J1 = 8.4, J2 = 902, H4a), 1.38 (2H, m, H2'a), 1.15 (2H, m, H2'b), 0.86 (2H, m, H2'c), 0.84 (3H, m, H2'd). **^{13}C NMR (100 MHz, DMSO-d_6) δ/ppm**: 196.8 (2M-CO, Cquat.), 187.6 (M-CO, Cquat.), 154.0 (C5, Cquat.), 153.6 (C1'", Cquat.), 151.7 (C1", Cquat.), 149.3 (C2', Cquat.), 143.6 (C4", Cquat.), 133.8 (C4'", Cquat.), 131.0 (C5', Cquat.), 127.1 (C2",6", -CH), 123.1 (C3",5", -CH), 123.0 (C4', Cquat.), 117.9 (C3'",5'", -CH), 111.4 (C2'",6'", −CH), 56.0 (C3, −CH), 30.7 (C4, −CH_2), 30.0 (C2'a, −CH_2), 28.3 (C2'b, -CH_2), 22.1 (C2'c, -CH_2)14.1 (C2'd, -CH_3). [**Total signal observed** = 20: signal of C = 10 (M-CO = 2, phenyl ring-C = 4, pyrazoline = 1, imidazole ring-C = 3), signal of -CH = 05 (pyrazoline -CH = 1, phenyl ring -CH = 4), signal of −CH_2 = 04 (pyrazoline −CH_2 = 1, imidazole −CH_2 = 3), -CH_3 = 1]. **IR Spectra** (KBr, 4000–400 cm^{-1}): 3278 ν(-NH)stret., 2931 ν(-CH)stret. alkane, 2862 ν(= CH)stret., 2361 ν(-C-N)stret., 1890, 2013 ν(M-CO), 1596, 1496 ν(C = N), 1249 ν(C = C)stret., 1026, 817 ν(para substitution), 617, 640 ν(C-Cl), 570 ν(Re-N).

4.4.5 Synthesis of [Re(CO)$_3$(L^5)Cl] (V)

It was synthesized using ligand (**L^5**) (0.316 g, 1.0 mmol). Yield: 85%; Color: brown crystalline solid; **m.p.**: 384°C; **Mol. wt.**: 842.38 g/mol **Empirical formula**: $C_{25}H_{21}Br_2Cl_2N_4O_3Re$; **Elemental analysis**: **Calc. (%)**: C, 35.65; H, 2.51; N, 6.65; Re, 22.10; **Found (%)**:C, 35.61; H, 2.48; N, 6.62; Re, 22.08. **Conductance**: 13.20 $ohm^{-1}cm^2mol^{-1}$. **^{1}H NMR (400 MHz, DMSO-d_6) δ/ppm**: 12.32 (1H, s, -NH), 7.98 (2H, d, J = 7.6 Hz, H2",6"), 7.66 (2H, d, J = 8.0 Hz, H3",5"), 7.39 (2H, d, J = 7.6 Hz, H2'",6'"), 7.26 (2H, d, J = 8.8 Hz, H3'",5'"), 5.30 (1H, dd, J1 =

6.0, J2 = 9.6, H3), 3.85 (1H, dd, J1 = 6.8 Hz, J2 = 10.8, H4b), 3.20 (1H, dd, J1 = 8.4, J2 = 9.2, H4a), 1.64 (2H, m, H2'a), 1.34 (2H, m, H2'b), 0.95 (2H, m, H2'c), 0.83 (3H, m, H2'd). **^{13}C NMR (100 MHz, DMSO-d_6) δ/ppm**: 183.7 (2M-CO, Cquat.), 182.5 (M-CO, Cquat.), 148.9 (C5, Cquat.), 148.3 (C2', Cquat.), 144.1 (C1‴, Cquat.), 143.5 (C1", Cquat.), 141.5 (C5', Cquat.), 139.0 (C4", Cquat.), 136.0 (C4', Cquat.), 129.7 (C3‴,5‴, -CH), 129.1 (C3",5", -CH), 126.3 (C2",6", -CH), 123.0 (C4‴, Cquat.), 114.9 (C2‴,6‴, CH), 55.0 (C3, −CH), 30.2 (C4, $-CH_2$), 28.9 (C2'a, $-CH_2$), 28.0 (C2'b, $-CH_2$), 22.0 (C2'c, $-CH_2$), 14.1 (C2'd, $-CH_3$). [**Total signal observed** = 20: signal of C = 10 (M-CO = 2, phenyl ring-C = 4, pyrazoline = 1, imidazole ring-C = 3), signal of -CH = 05 (pyrazoline -CH = 1, phenyl ring -CH = 4), signal of $-CH_2$ = 04 (pyrazoline $-CH_2$ = 1, imidazole $-CH_2$ = 3), $-CH_3$ = 1]. **IR Spectra** (KBr, 4000–400 cm^{-1}): 3278 ν(-NH)stret., 2954 ν(-CH)stret. alkane, 2862 ν(= CH)stret., 2360 ν(-C-N)stret., 1890, 2013 ν(M-CO), 1589, 1488 ν(C = N), 1249 ν(C = C)stret., 1072, 817 ν(para substitution), 617, 640 ν(C-Cl), 570 ν(Re-N).

4.4.6 Synthesis of $[Re(CO)_3(L^6)Cl]$ (VI)

It was synthesized using ligand (**L^6**) (0.316 g, 1.0 mmol). Yield: 86%; Color: brown crystalline solid; **m.p.**: 378°C; **Mol. wt.**: 774.67 g/mol; **Empirical formula**: $C_{28}H_{29}Cl_2N_4O_6Re$; **Elemental analysis**: **Calc. (%)**: C, 43.41; H, 3.77; N, 7.23; Re, 24.04; **Found (%)**: C, 43.37; H, 3.75; N, 7.20; Re, 24.01. **Conductance**: 17.60 $ohm^{-1}cm^2mol^{-1}$. **^{1}H NMR (400 MHz, DMSO-d_6) δ/ppm**: 12.26 (1H, s, -NH), 7.83 (2H, d, J = 8.0 Hz, H2",6"), 7.65 (1H, d, J = 8.4 Hz, H5"), 7.37 (2H, d, J = 8.8 Hz, H2‴,6‴), 6.98 (2H, d, J = 8.4 Hz, H3‴,5‴), 5.36 (1H, dd, J1 = 8.0, J2 = 12.4, H3), 4.10 (9H, s, 3-OCH_3), 3.85 (1H, dd, J1 = 4.8 Hz, J2 = 9.6, H4b), 3.22 (1H, dd, J1 = 8.0, J2 = 9.6, H4a), 1.54 (2H, m, H2'a), 1.35 (2H, m, H2'b), 0.96 (2H, m, H2'c), 0.84 (3H, m, H2'd). **^{13}C NMR (100 MHz, DMSO-d_6) δ/ppm**: 190.5 (2M-CO, Cquat.), 186.8(M-CO, Cquat.), 162.5 (C5, Cquat.), 161.2 (C4‴, Cquat.), 153.7 (C4", Cquat.), 151.7 (C3", Cquat.), 149.4 (C2', Cquat.), 141.6 (C1‴, Cquat.), 138.5 (C1", Cquat.), 131.1 (C5', Cquat.), 127.1 (C6", -CH), 123.1 (C2", -CH), 123.1 (C4', Cquat.), 117.9 (C5", −CH), 111.4 (C3‴,5‴, -CH), 110.9 (C2‴,6‴, -CH), 56.3 (-OCH_3), 56.2 (-OCH_3), 56.0 (-OCH_3), 53.2 (C3, -CH), 30.1 (C4, $-CH_2$), 30.0 (C2'a, $-CH_2$), 28.3 (C2'b, $-CH_2$), 22.1 (C2'c, $-CH_2$). 14.1 (C2'd, $-CH_3$). [**Total signal observed** = 25: signal of C = 11 (M-CO = 2, phenyl ring-C = 3, pyrazoline = 1, imidazole ring-C = 3), signal of -CH = 06 (pyrazoline -CH = 1, phenylring -CH = 5), signal of $-CH_2$ = 04 (pyrazoline $-CH_2$ = 1, imidazole $-CH_2$ = 3), $-CH_3$ = 1, -OCH_3 = 3]. **IR Spectra** (KBr, 4000–400 cm^{-1}): 3278 ν(-NH)stret., 2931 ν(-CH)stret. alkane, 2869 ν(= CH)stret., 2360 ν(-C-N)stret., 2013, 1890 ν(M-CO), 1589, 1512 ν(C = N), 1249 ν(C = C)stret., 1026, 825 ν(para substitution), 617, 640 ν(C-Cl), 578 ν(Re-N).

4.5 Biological activities

4.5.1 Cytotoxicity on S. cerevisiae cells

The cellular level bioassay was carried out using *S. cerevisiae* cells [31]. The cells were grown in 50 mL yeast extract media in 150 mL Erlenmeyer flask. The flask was incubated at 30 ^oC on a shaker at 150 rpm till the exponential growth of *S. cerevisiae* obtained (24 to 30 h). The cell culture was treated with different concentrations (2, 4, 6, 8, 10 $mgmL^{-1}$) of complexes, free ligands and DMSO (control), and

incubated for 16–18 h. Next day, the treated cells were collected by centrifugation at 10,000 rpm for 10 min and were dissolved in 500 mL of PBS. The 80 mL of yeast culture dissolved in PBS and 20 mL of 0.4% trypan blue prepared in PBS were mixed, and cells were observed in a compound microscope (40X). The dye could enter the dead cell only, so they appeared blue whereas live cells resisted the entry of dye. The number of dead cells and the number of live cells were counted.

4.5.2 In vivo cytotoxicity

The cytotoxicity of complexes was studied on brine shrimp, *Artemia cysts*, according to the reported method [32]. In this experiment, 10 nauplii (larvae) were added to the vials of 24-well Microtiter plate with a total volume of to 2500 µL per vial [1450 µL sea salt solution + 1000 µL sea salt containing 10 nauplii + + 50 µL (complex + DMSO)], [DMSO] < 2 % (V/V). After 24 h of incubation, live and dead larvae were counted and the LC_{50} values were determined for each complex [33].

4.5.3 In vitro antibacterial activity

The *in vitro* antibacterial activity of ligands, complexes and standard drug, gatifloxacin was performed according to the literature procedure [34]. Luria Broth was used as the bacteria growth medium. Serially diluted concentrations of each of test compounds (in DMSO) from 20 to 2800 µM were prepared for the determination of MIC and vaccinated with five different microorganisms. The solution without turbidity was noted as the minimum inhibitory concentration after overnight incubation at 37 ^{o}C.

4.5.4 Reactive oxygen species (ROS)

The amount of H_2O_2 was quantified as described by Loreto and Velikova [35]. In the process, treated cultures centrifuged at 5000 rpm for 5 min, was used for H_2O_2 determination. The reaction system consist of 0.5 mL supernatant was added to 0.5 ml of 10 mM phosphate buffer (pH 7.0) and 1.0 mL of 1 M KI. After completion of reaction, absorbance was measured at 390 nm and results were expressed as µg/mL H_2O_2 of culture.

4.5.5 Lipid Peroxidation

For the measurements of lipid peroxidation in *Saccharomyces cerevisiae*, the thiobarbituric acid (TBA) test, which determines MDA as an end product of lipid peroxidation was used [36]. We combined 1.0 mL of biological sample {0.1-2.0 mg of membrane protein or 0.1–0.2 /µmol of lipid phosphate} with 2.0 ml of TCA-TBA-HCl and mixed it thoroughly. The solution was heated for 15 min in a boiling water bath. After cooling, the flocculent precipitates were removed by centrifugation at 1000 rpm for 10 min. The absorbance of the sample was determined at 535 nm against a blank that contains all the reagents minus the lipid. The malondialdehyde concentration of the sample was calculated using an extinction coefficient of $1.56 \times 10 \sim M^{-1}\ cm^{-l}$ [37].

4.5.6 Antiproliferative study

Stock solutions of 10–100 mg/mL of test complexes (I-VI) were prepared in dimethyl sulfoxide (DMSO). HCT 116 cells were cultured in RPMI 1640 medium. The culture media were supplemented with 10% fetal

bovine serum and an antibiotic cocktail containing penicillin (5mg/ml), streptomycin (5 mg/mL) and neomycin (10 mg/mL). The cells were cultured in a humidified atmosphere of 5% CO_2 at 37°C. The entire study was executed using exponentially growing cells. Twenty-four hours after cell plating, media was removed and replaced with fresh media containing 10, 25, 50, 100, 500 µg/mL of test compounds DMSO vehicle control, for the indicated exposure times. The Re(I) tricarbonyl complexes I-VI were tested for their *in vitro* cytotoxicity against colon carcinoma (HCT116) cancerous cell lines. The MTT (3-(4,5-dimethylthiazol-2-yl)-2,5-diphenyltetrazolium bromide) assay was used to determine the cytotoxicity of the compounds. The extent of inhibition is displayed as an IC_{50} value, which is defined as the concentration required to inhibit cell growth to half [38].

4.5.7 DNA interaction

Absorption spectral analysis

In this experiment, fixed amount of DNA solution (100 µL) in phosphate buffer was added to sample cell holding in definite concentration of complex solution (20 µmol L^{-1}) and reference cell to nullify the effect of HS DNA, and allowed to incubate for 10 min prior to the spectra being recorded. DMSO was also added into the reference cell as a control to nullify the effect of DMSO.

Hydrodynamic volume measurement

Viscometric experiments were performed using Ubbelohde viscometer, maintained at 25.0 (± 0.5) °C in a thermostatic water bath. The concentration of DNA was 100 µM and that of metal complex was varied from 5 to 50 µM. Flow time of solutions in phosphate buffer (pH 7.0) was recorded in triplicate for each sample, and an average flow time was calculated. The hydrodynamic length of DNA generally increases upon partial intercalation while it does not lengthen upon groove binding [39].

Molecular docking with DNA sequence d(ACCGACGTCGGT) $_2$

To determine the theoretical binding energy of synthesized compounds to DNA, docking study was performed using HEX 6.0 software [40]. The .pdb files of complex coordinates were obtained by converting their .mol file using CHIMERA 1.5.1 software. The structure of B-DNA (1 BNA: 5'-D(*CP*GP*CP*GP*AP*TP*TP*CP*GP*CP*G)-3') obtained from the Protein Data Bank (http://www.rcsb.org/pdb). All solvents were removed before docking. Grid dimension 0.6 with FFT mode 3D and correlation type shape only were used. The other parameters kept at their default values.

Agarose gel electrophoresis: photo quantization technique

Effect of compounds on the integrity of DNA of *S. cerevisiae* cells results of cytotoxicity encouraged us to find out whether the compounds have any effect on the integrity of DNA. DNA extraction of *S. cerevisiae* yeast was carried out according to the process given in literature [41, 42].

Declarations

ACKNOWLEDGEMENTS

The authors are thankful to the Head, Department of Chemistry, Sardar Patel University, Vallabh Vidyanagar, Gujarat, India, for providing necessary research facilities, Sardar Patel University, Vallabh Vidyanagar, CPEPA, UGC, New Delhi for providing chemicals facility, DST-PURSE Sardar Patel University, Vallabh Vidyanagar for LC-MS analysis.

CONFLICT OF INTEREST

Authors declare no conflict of interest.

References

[1] A.M.F. Phillips, A.J. Pombeiro, Tansition Metal-Based Prodrugs for Anticancer Drug Delivery, Current medicinal chemistry (2019).

[2] L.H. Abdel-Rahman, A.M. Abu-Dief, R.M. El-Khatib, S.M. Abdel-Fatah, Some new nano-sized Fe (II), Cd (II) and Zn (II) Schiff base complexes as precursor for metal oxides: Sonochemical synthesis, characterization, DNA interaction, in vitro antimicrobial and anticancer activities, Bioorganic chemistry 69 (2016) 140-152.

[3] Y.-M. Sun, W. Akram, F. Cheng, Z.-Y. Liu, Y.-H. Liao, Y. Ye, H.-Y. Liu, DNA interaction and photodynamic antitumor activity of transition metal mono-hydroxyl corrole, Bioorganic chemistry 90 (2019) 103085.

[4] F. Özen, A. Günel, A. Baran, DNA-binding, enzyme inhibition, and photochemical properties of chalcone-containing metallophthalocyanine compounds, Bioorganic chemistry 81 (2018) 71-78.

[5] S.B. Kavukcu, O. Şahin, H.S. Vatansever, F.O. Kurt, M. Korkmaz, R. Kendirci, L. Pelit, H. Türkmen, Synthesis and Cytotoxic Activities of Organometallic Ru (II) Diamine Complexes, Bioorganic Chemistry (2020) 103793.

[6] B.E. Mann, Carbon monoxide: an essential signalling molecule, Medicinal Organometallic Chemistry, Springer2010, pp. 247-285.

[7] R. Motterlini, L.E. Otterbein, The therapeutic potential of carbon monoxide, Nature reviews Drug discovery 9(9) (2010) 728.

[8] F. Zobi, O. Blacque, R.A. Jacobs, M.C. Schaub, A.Y. Bogdanova, 17 e− rhenium dicarbonyl CO-releasing molecules on a cobalamin scaffold for biological application, Dalton Transactions 41(2) (2012) 370-378.

[9] C.C. Romao, W.A. Blättler, J.D. Seixas, G.J. Bernardes, Developing drug molecules for therapy with carbon monoxide, Chemical Society Reviews 41(9) (2012) 3571-3583.

[10] T.R. Johnson, B.E. Mann, J.E. Clark, R. Foresti, C.J. Green, R. Motterlini, Metal carbonyls: a new class of pharmaceuticals?, Angewandte Chemie International Edition 42(32) (2003) 3722-3729.

[11] U. Abram, R. Alberto, Technetium and rhenium: coordination chemistry and nuclear medical applications, Journal of the Brazilian Chemical Society 17(8) (2006) 1486-1500.

[12] M. Antolini, A. Bozzoli, C. Ghiron, G. Kennedy, T. Rossi, A. Ursini, Analogues of 4, 5-bis (3, 5-dichlorophenyl)-2-trifluoromethyl-1H-imidazole as potential antibacterial agents, Bioorganic & medicinal chemistry letters 9(7) (1999) 1023-1028.

[13] R.R. Varma, B.H. Pursuwani, E. Suresh, B.S. Bhatt, M.N. Patel, Single crystal, DNA interaction and cytotoxicity studies of rhenium (I) organometallic compounds, Journal of Molecular Structure 1200 (2020) 127068.

[14] A. Karaküçük-İyidoğan, D. Taşdemir, E.E. Oruç-Emre, J. Balzarini, Novel platinum(II) and palladium(II) complexes of thiosemicarbazones derived from 5-substitutedthiophene-2-carboxaldehydes and their antiviral and cytotoxic activities, European Journal of Medicinal Chemistry 46(11) (2011) 5616-5624.

[15] K. Chanawanno, J.T. Engle, K.X. Le, R.S. Herrick, C.J. Ziegler, The synthesis and pH-dependent behaviour of Re (CO) 3 conjugates with diimine phenolic ligands, Dalton Transactions 42(37) (2013) 13679-13684.

[16] G. Balakrishnan, T. Rajendran, K.S. Murugan, M.S. Kumar, V.K. Sivasubramanian, M. Ganesan, A. Mahesh, T. Thirunalasundari, S. Rajagopal, Interaction of rhenium (I) complex carrying long alkyl chain with Calf Thymus DNA: Cytotoxic and cell imaging studies, Inorganica Chimica Acta 434 (2015) 51-59.

[17] G. Zhao, Y. Hui, J.K. Rupprecht, J.L. McLaughlin, K.V. Wood, Additional bioactive compounds and trilobacin, a novel highly cytotoxic acetogenin, from the bark of Asimina triloba, Journal of Natural Products 55(3) (1992) 347-356.

[18] B. Tweedy, Plant extracts with metal ions as potential antimicrobial agents, Phytopathology 55 (1964) 910-914.

[19] F.L. Thorp-Greenwood, M.P. Coogan, L. Mishra, N. Kumari, G. Rai, S. Saripella, The importance of cellular localisation of probes: synthesis, photophysical properties, DNA interactions and cellular imaging properties of rhenium dppz complexes with known cellular localisation vectors, New Journal of Chemistry 36(1) (2012) 64-72.

[20] B. Lippert, Multiplicity of metal ion binding patterns to nucleobases, Coordination Chemistry Reviews 200 (2000) 487-516.

[21] H.-K. Liu, P.J. Sadler, Metal complexes as DNA intercalators, Accounts of Chemical Research 44(5) (2011) 349-359.

[22] M.L. Kopka, C. Yoon, D. Goodsell, P. Pjura, R.E. Dickerson, Binding of an antitumor drug to DNA: netropsin and CGCGAATT-BrC-GCG, Journal of molecular biology 183(4) (1985) 553-563.

[23] S.S. Mati, S.S. Roy, S. Chall, S. Bhattacharya, S.C. Bhattacharya, Unveiling the groove binding mechanism of a biocompatible naphthalimide-based organoselenocyanate with calf thymus DNA: an “ex vivo” fluorescence imaging application appended by biophysical experiments and molecular docking simulations, The Journal of Physical Chemistry B 117(47) (2013) 14655-14665.

[24] B. Nordén, F. Tjerneld, Structure of methylene blue–DNA complexes studied by linear and circular dichroism spectroscopy, Biopolymers: Original Research on Biomolecules 21(9) (1982) 1713-1734.

[25] A.K. Patra, T. Bhowmick, S. Roy, S. Ramakumar, A.R. Chakravarty, Copper (II) complexes of L-arginine as netropsin mimics showing DNA cleavage activity in red light, Inorganic chemistry 48(7) (2009) 2932-2943.

[26] R. Bera, B.K. Sahoo, K.S. Ghosh, S. Dasgupta, Studies on the interaction of isoxazolcurcumin with calf thymus DNA, International journal of biological macromolecules 42(1) (2008) 14-21.

[27] Y. Gilad, H. Senderowitz, Docking studies on DNA intercalators, Journal of chemical information and modeling 54(1) (2013) 96-107.

[28] D. Shao, M. Shi, Q. Zhao, J. Wen, Z. Geng, Z. Wang, Synthesis, Crystal Structure, DNA Binding, Cleavage and Docking Studies of a Novel Dinuclear Schiff-Base Copper (II) Complex, Zeitschrift für anorganische und allgemeine Chemie 641(2) (2015) 454-459.

[29] A. Pyle, J. Rehmann, R. Meshoyrer, C. Kumar, N. Turro, J.K. Barton, Mixed-ligand complexes of ruthenium (II): factors governing binding to DNA, Journal of the American Chemical Society 111(8) (1989) 3051-3058.

[30] A. Guida, M.H. Lhouty, D. Tichit, F. Figueras, P. Geneste, Hydrotalcites as base catalysts. Kinetics of Claisen-Schmidt condensation, intramolecular condensation of acetonylacetone and synthesis of chalcone, Applied Catalysis A: General 164(1-2) (1997) 251-264.

[31] K.P. Thakor, M.V. Lunagariya, B.S. Bhatt, M.N. Patel, Fluorescence and absorption titrations of bio-relevant imidazole based organometallic Pd (II) complexes with DNA: synthesis, characterization, dna interaction, antimicrobial, cytotoxic and molecular docking studies, Journal of Inorganic and Organometallic Polymers and Materials (2019) 1-12.

[32] B.N. Meyer, N.R. Ferrigni, J.E. Putnam, L.B. Jacobsen, D.E. Nichols, J.L. McLaughlin, Brine shrimp: a convenient general bioassay for active plant constituents, Planta Med. 45(5) (1982) 31-4.

[33] M.N. Patel, B.S. Bhatt, P.A. Dosi, N.V. Amaravady, H.V. Movaliya, Synthesis, spectral investigation and biological interphase of drug-based cytotoxic square pyramidal coordination compounds, Applied Organometallic Chemistry 26(5) (2012) 217-224.

[34] M.N. Patel, B.S. Bhatt, P.A. Dosi, Topoisomerase inhibition, nucleolytic and electrolytic contribution on DNA binding activity exerted by biological active analogue of coordination compounds, Applied biochemistry and biotechnology 166(8) (2012) 1949-1968.

[35] F. Loreto, V. Velikova, Isoprene produced by leaves protects the photosynthetic apparatus against ozone damage, quenches ozone products, and reduces lipid peroxidation of cellular membranes, Plant Physiology 127(4) (2001) 1781-1787.

[36] R.L. Heath, L. Packer, Photoperoxidation in isolated chloroplasts: I. Kinetics and stoichiometry of fatty acid peroxidation, Archives of biochemistry and biophysics 125(1) (1968) 189-198.

[37] J.A. Buege, S.D. Aust, [30] Microsomal lipid peroxidation, Methods in enzymology, Elsevier1978, pp. 302-310.

[38] P. Zou, S. Yuan, X. Yang, X. Zhai, J. Wang, Chitosan oligosaccharides with degree of polymerization 2–6 induces apoptosis in human colon carcinoma HCT116 cells, Chemico-biological interactions 279 (2018) 129-135.

[39] F. Leng, W. Priebe, J.B. Chaires, Ultratight DNA binding of a new bisintercalating anthracycline antibiotic, Biochemistry 37(7) (1998) 1743-1753.

[40] K.P. Thakor, M.V. Lunagariya, B.S. Bhatt, M.N. Patel, Fluorescence and absorption studies of DNA–Pd (II) complex interaction: Synthesis, spectroanalytical investigations and biological activities, Luminescence 34(1) (2019) 113-124.

[41] J. Sambrook, D.W. Russell, Rapid isolation of yeast DNA, Cold Spring Harbor Protocols 2006(1) (2006) pdb. prot4039.

[42] M.R. Green, J. Sambrook, Rapid isolation of yeast DNA, Cold Spring Harbor Protocols 2018(6) (2018) pdb. prot093542.

Figures

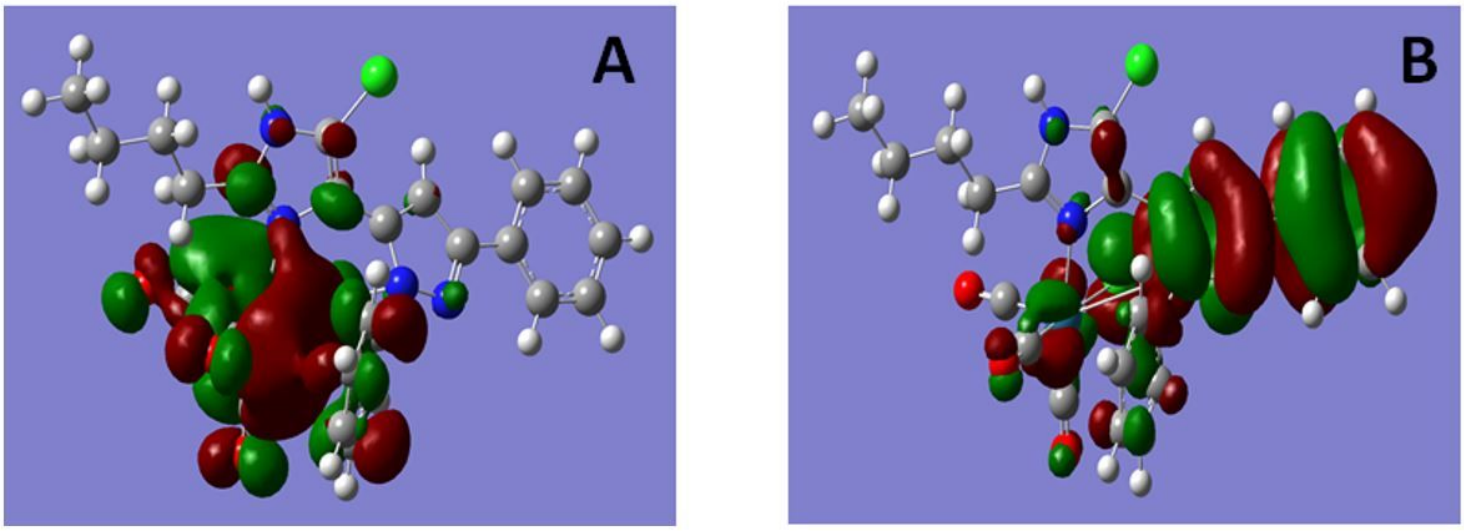


Figure 1

HOMO (A) and LUMO (B) orbital containing structures of the complex - I.

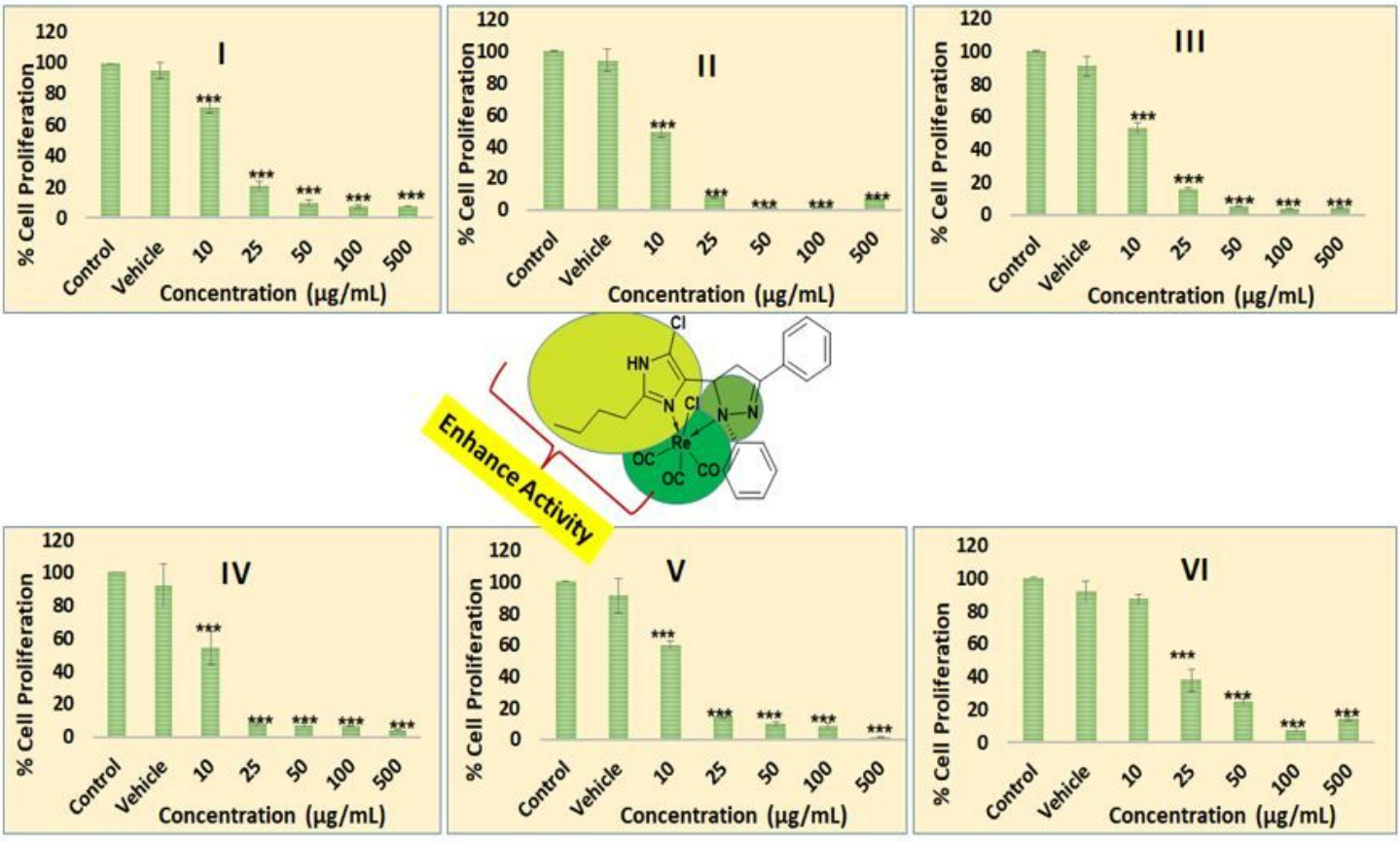


Figure 2

% cell proliferation of synthesised complexes (I-VI)

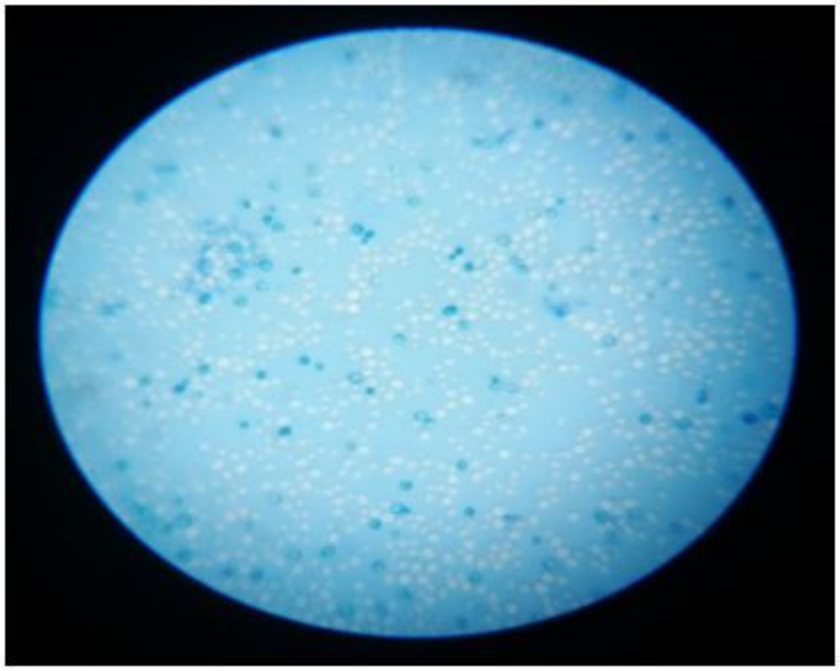


Figure 3

Effect of compounds on S. cerevisiae cells, dead cells are seen dark whereas live cells are seen transparent

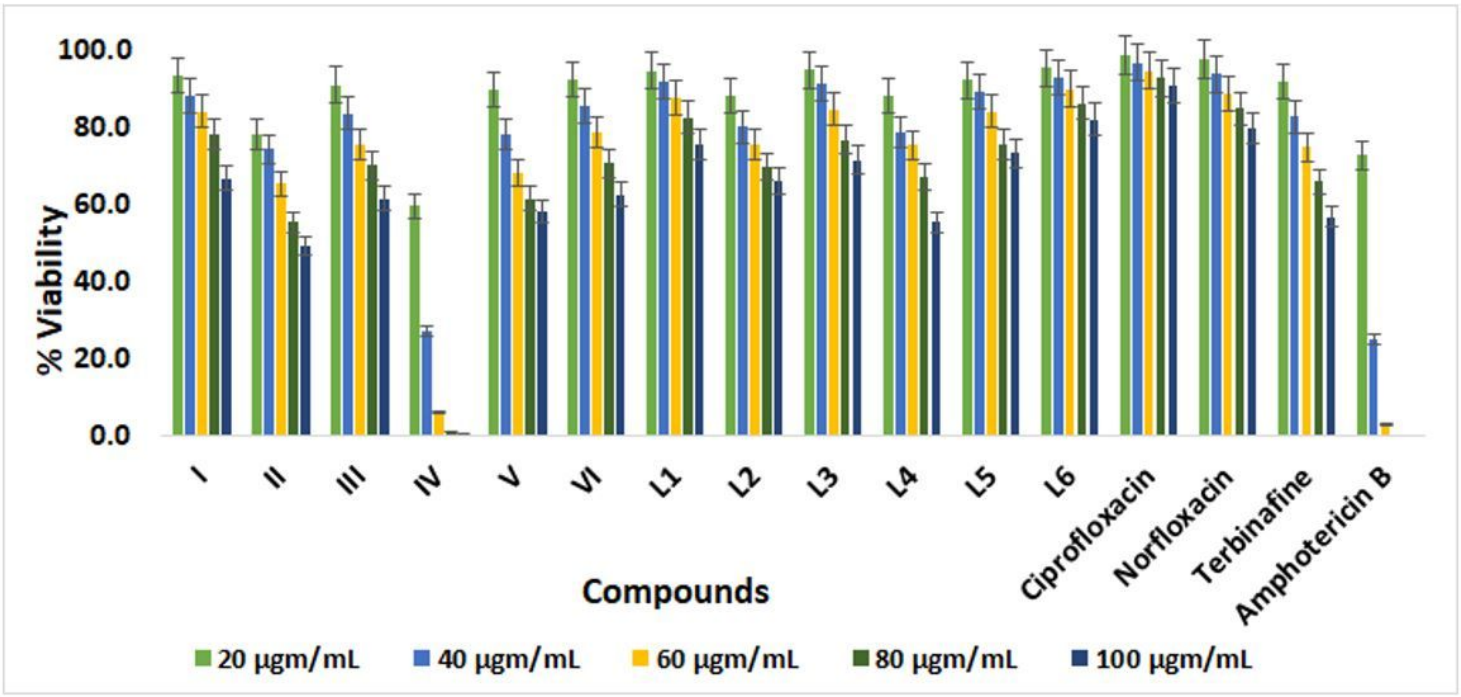


Figure 4

Effect of compounds on S. cerevisiae yeast cells

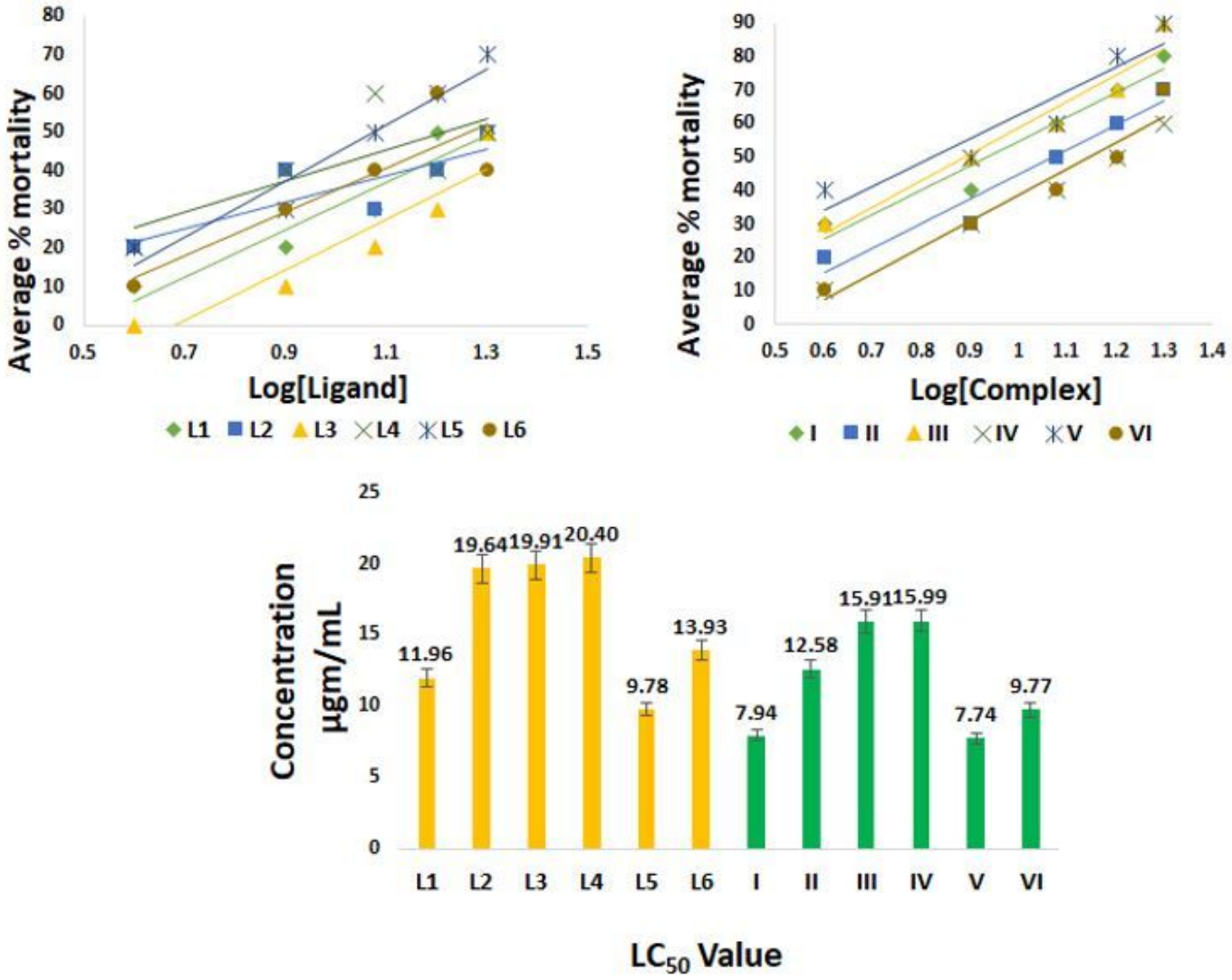


Figure 5

Plot of LC50 values of different compounds in µg/mL using Brine shrimp. A plot of log concentration versus percentage of mortality in linear correlation

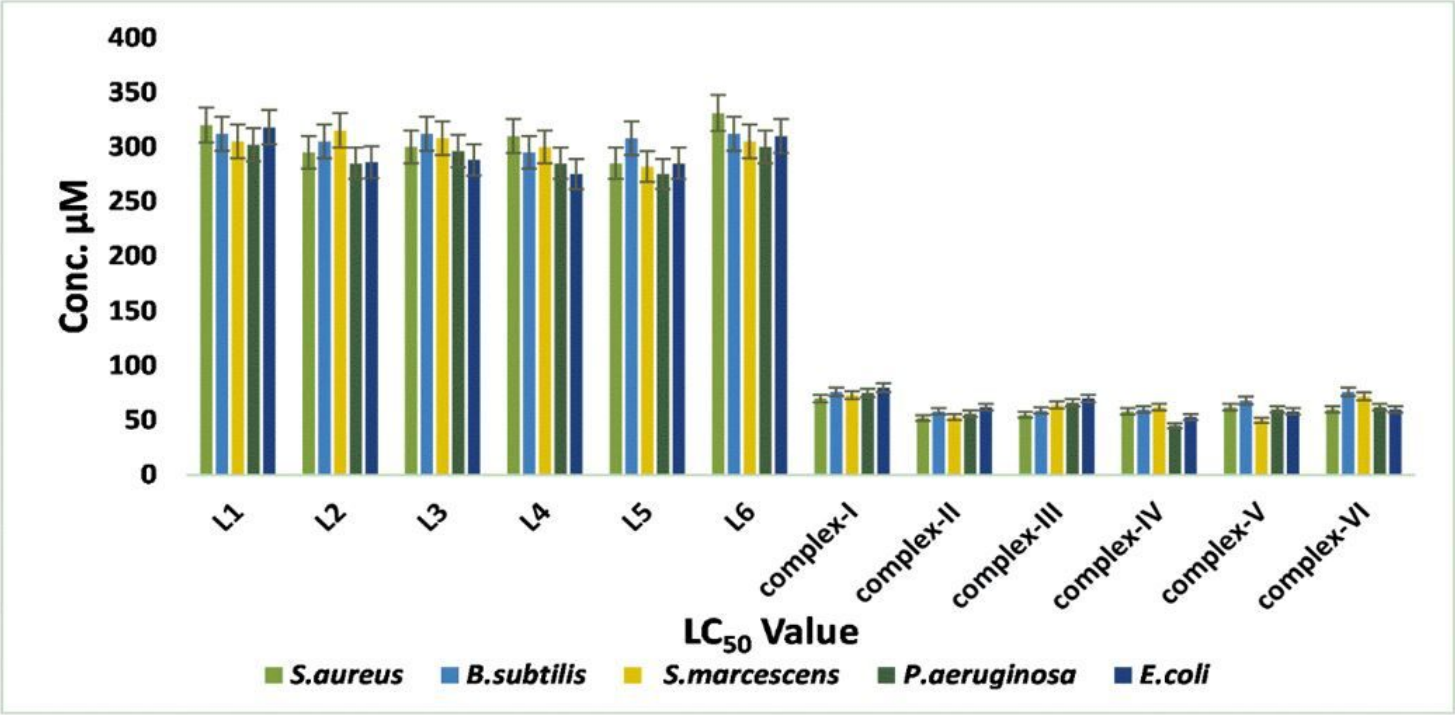


Figure 6

Effect of different concentrations (µM) ligands and their rhenium(I) complexes on two Gram(+ve) and three Gram(−ve) microorganisms

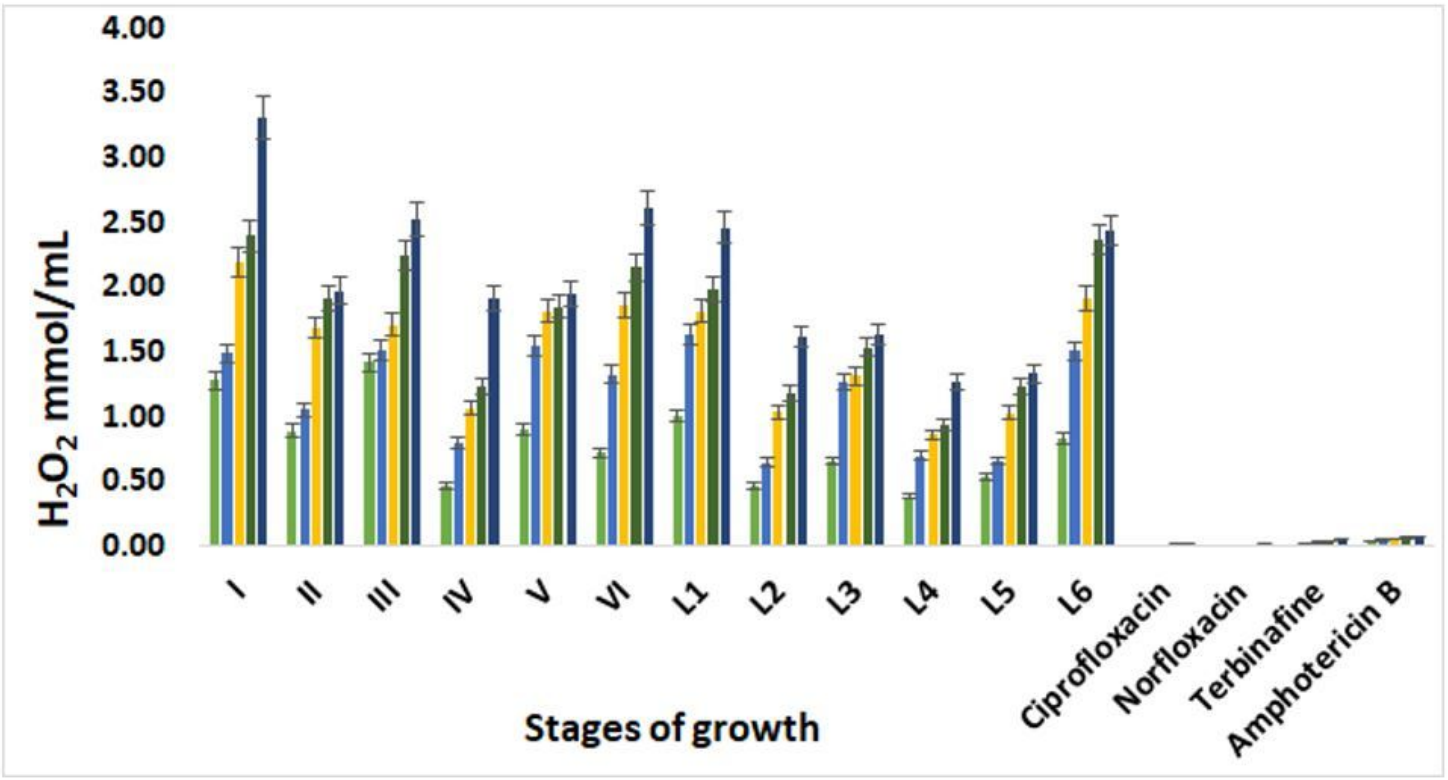


Figure 7

H2O2 accumulation in S. cerevices using ligands (L1-L6) and complexes (I-VI) with standard drugs

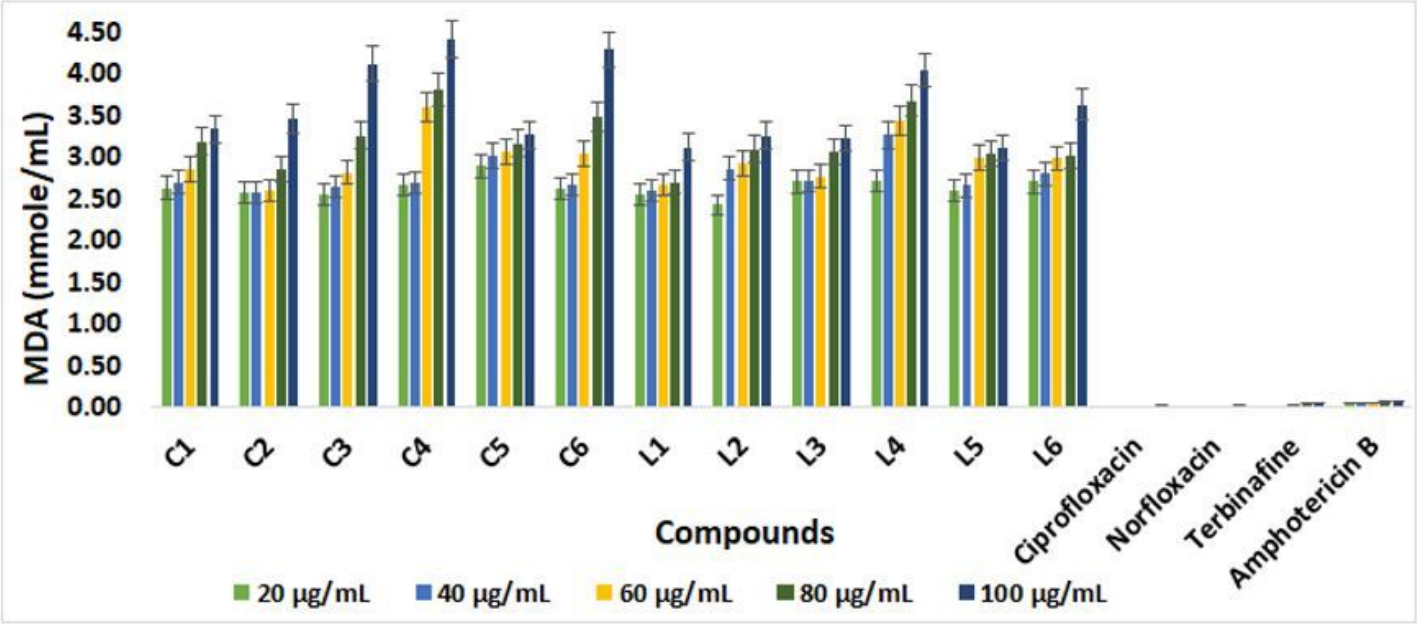


Figure 8

MDA production in S. cerevices yeast using ligands (L1-L6) and complexes (I-VI) with standard drugs

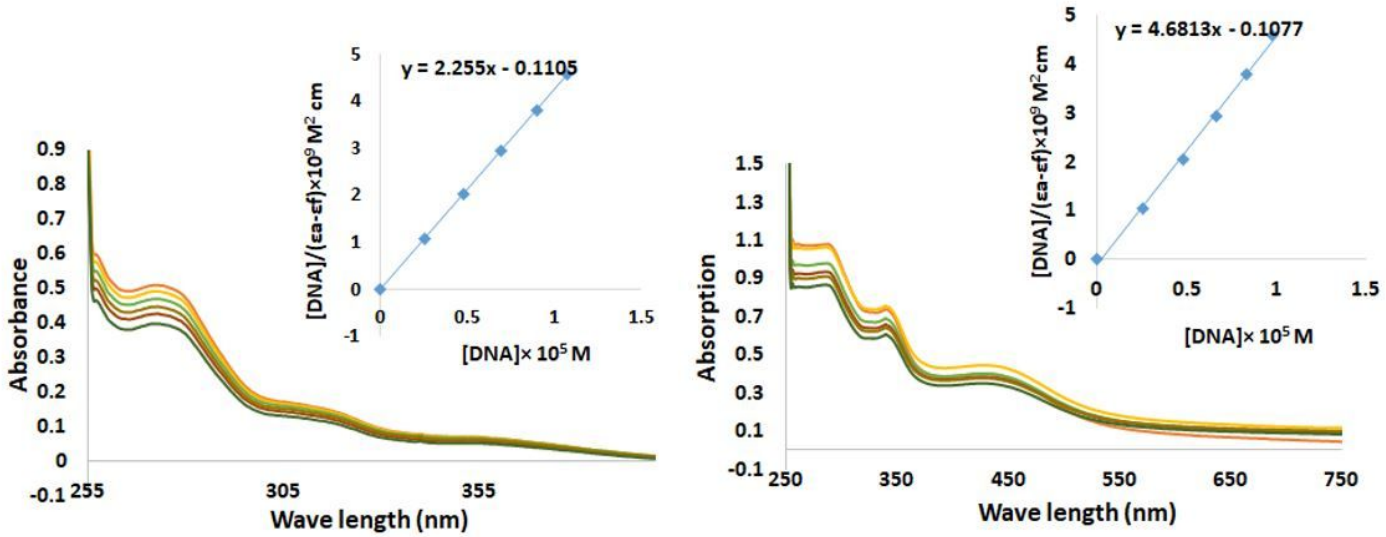


Figure 9

Absorption spectral changes on the addition of HS DNA to the solution of ligand (L1) and complex (I), after incubating it for 10 minutes at room temperature in phosphate buffer (Na2HPO4/NaH2PO4, pH = 7.2). Inset: plot of [DNA]/(εa − εf) vs. [DNA], the change in absorption with increase in concentration of DNA

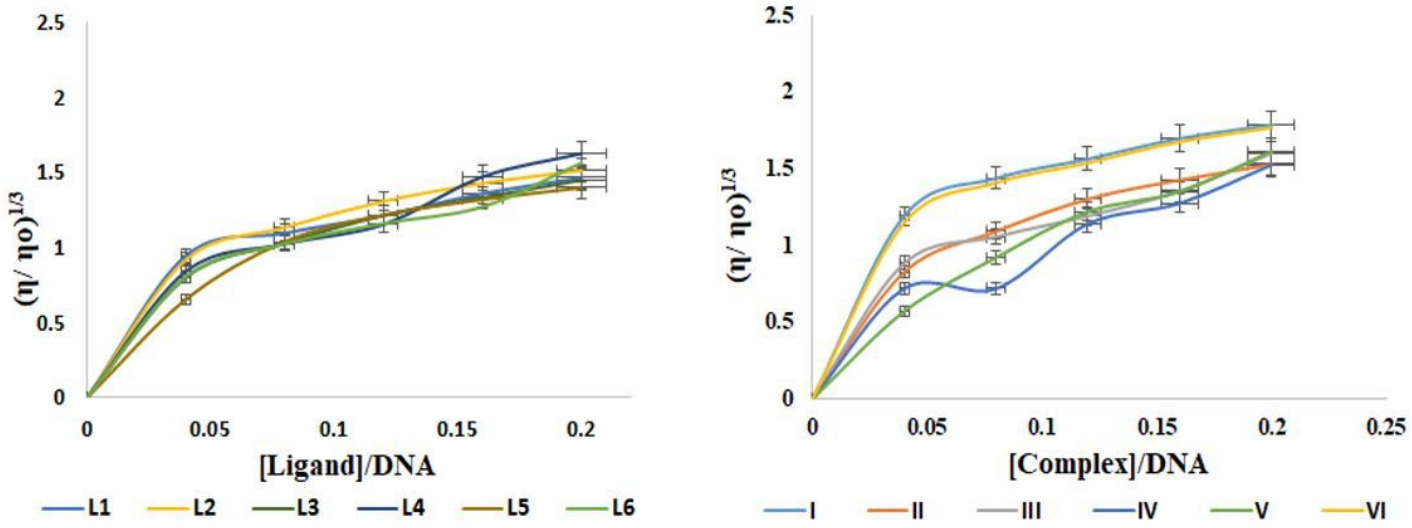


Figure 10

The effect of increasing amounts of complexes on the relative viscosity of HS DNA at 25 (±0.5) °C in phosphate buffer at pH = 7.2

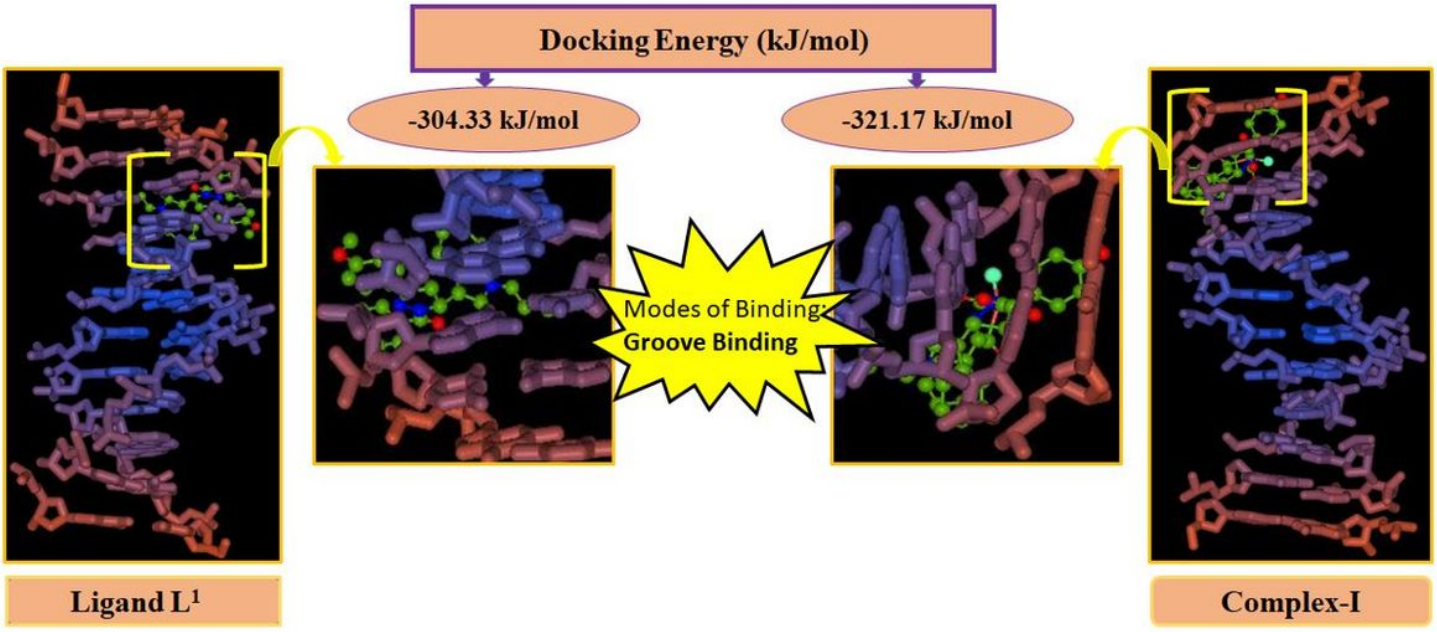


Figure 11

Molecular docking of ligand L1 and complex-I (ball and stick) with the DNA duplex (VDW spheres) of sequence d(ACCGACGTCGGT)2. The complex is docked inside the DNA groove

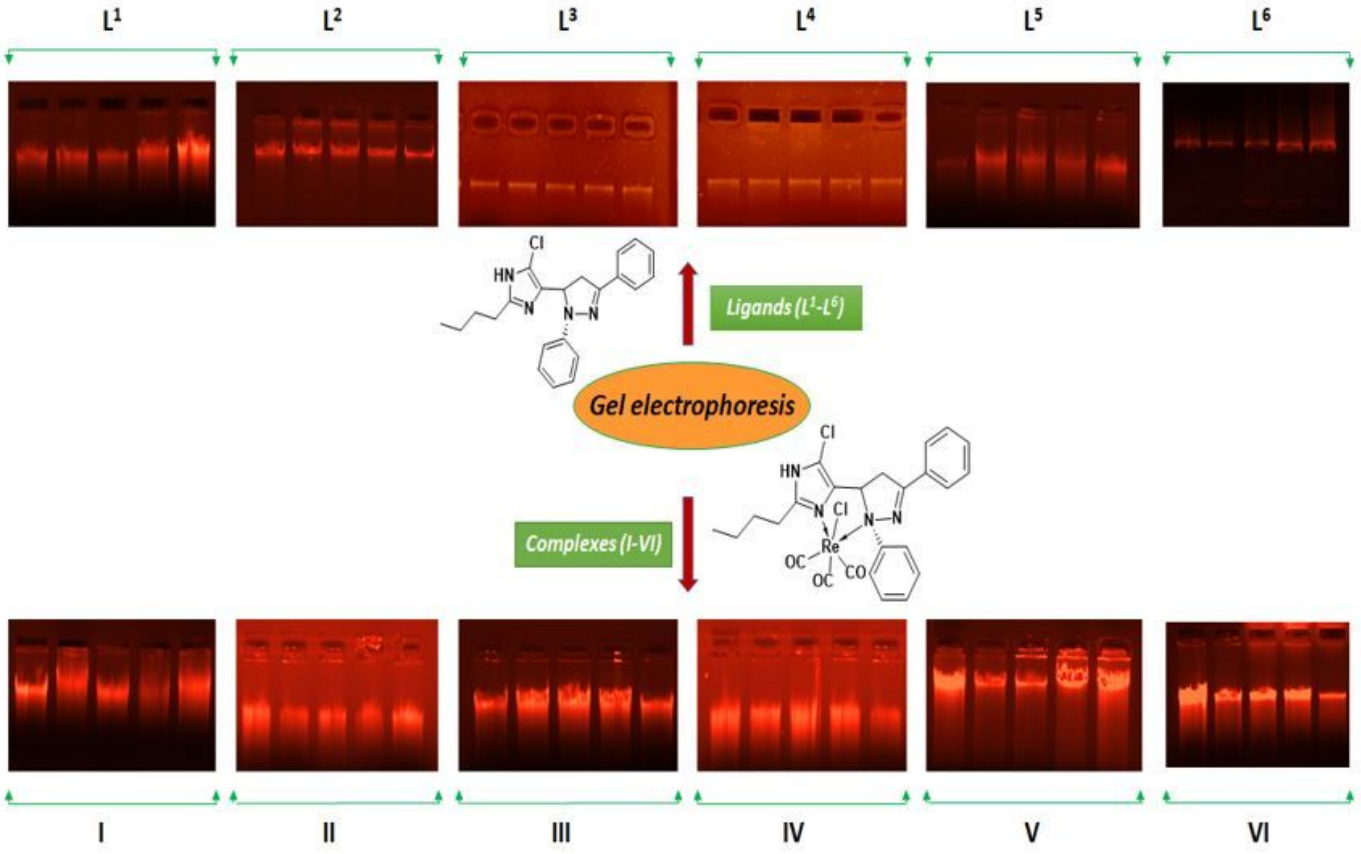
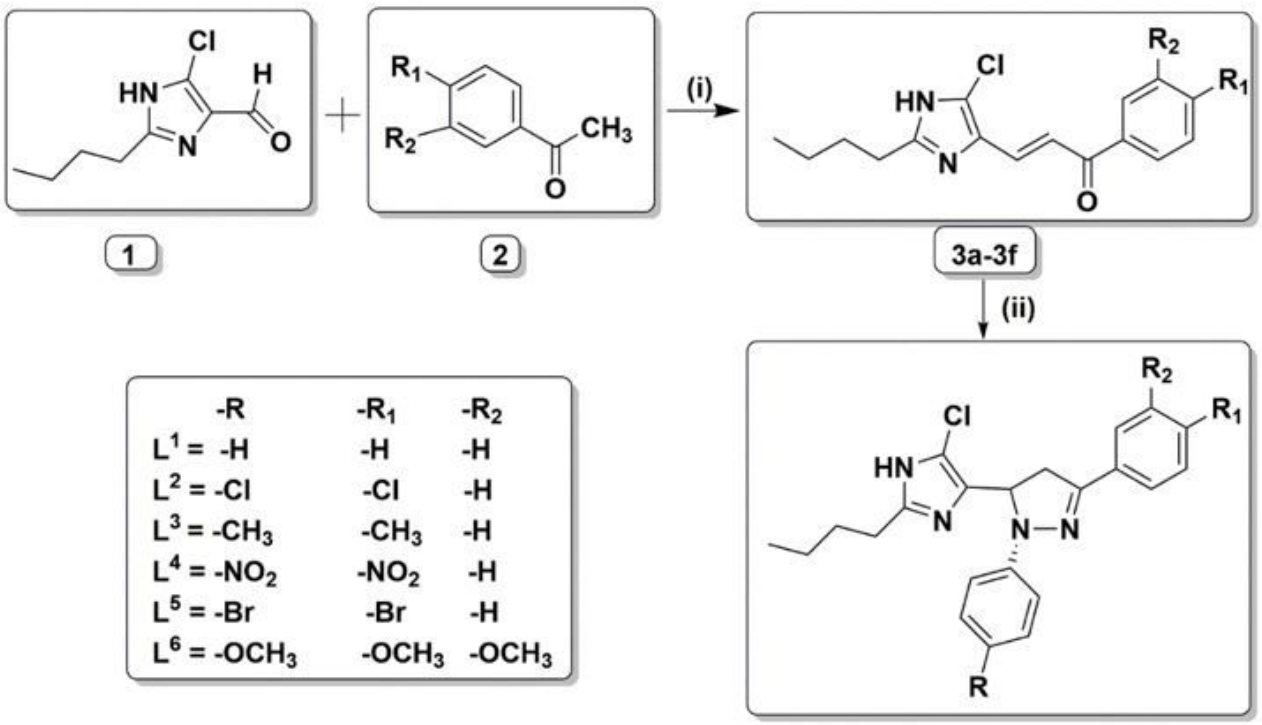


Figure 12

Photogenic view of the cleavage of S. cerevisiae DNA with a series of compounds using 1% agarose gel containing 0.5 μg cm−3 EtBr for 24 h at 37 °C



-R	$-R_1$	$-R_2$
L^1 = -H	-H	-H
L^2 = -Cl	-Cl	-H
L^3 = $-CH_3$	$-CH_3$	-H
L^4 = $-NO_2$	$-NO_2$	-H
L^5 = -Br	-Br	-H
L^6 = $-OCH_3$	$-OCH_3$	$-OCH_3$

Reagent and Conditions:

(i) Methanol, KOH

(ii) Ethanol, substituted phenyl hydrazine, K^tOBu, 70-90 °C

Figure 13

General reaction scheme for synthesis of ligands (L1-L6)

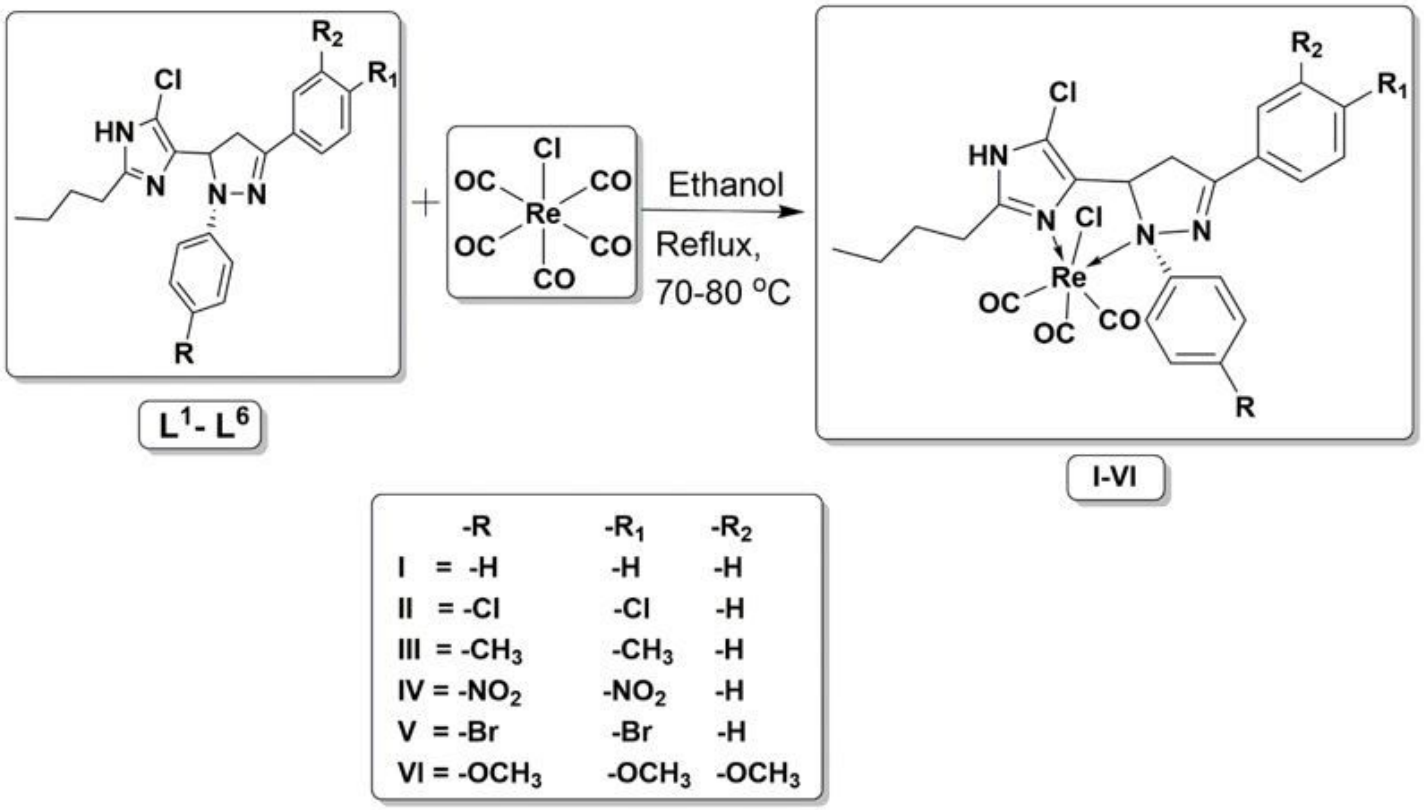


Figure 14

General reaction scheme for synthesis of complexes (I-VI)

Supplementary Files

This is a list of supplementary files associated with this preprint. Click to download.

- scheme1.jpg
- scheme2.jpg
- SupplementaryMaterial.docx